SYNTHESIS AND CHARACTERIZATION OF CHIRAL MIXED LIGAND NANOCLUSTERS AND NACRE-LIKE STRUCTURE

by

Zekiye Pelin Güven

Submitted to the Graduate School of Engineering and Natural Sciences

In partial fulfillment of the requirements for the degree of

Master of Science

Sabanci University

July, 2014

SYNTHESIS AND CHARACTERIZATION OF CHIRAL MIXED LIGAND NANOCLUSTERS AND NACRE-LIKE STRUCTURE

Zekiye Pelin Güven

MAT, Master of Science Thesis, 2014

Thesis Supervisor: Assist. Prof. Özge Akbulut

Keywords: Silver Nanoclusters, Chirality, Mixed Ligands, Nacre

Abstract

Nanoclusters gained attention due to their possible applications in biosensing, biolabeling, and optics. In this thesis we report the synthesis and characterization of mixed ligand silver nanoclusters that exhibit chiral behavior. We explored the occurrence of this behavior by changing the silver to thiol ratio, ratio of the ligands and using different ligands.

Nacre-like structures are of interest due to their toughness that goes far beyond ceramic materials. This toughness arises from the layered structure which is kept together by biomolecules such that when stress is applied, the layers slide and entering the brittle regime is postponed. In addition, cracks cannot propagate in nacre due to organic/inorganic layering. To fabricate nacre-like materials, organic and inorganic layers are coated via layer-by-layer assembly or *in situ* biomineralization in an organic matrix is used. In this thesis we synthesized nacre-like layered nano/meso building blocks in a controlled and easy manner by the reduction of silver salt in the presence of two different ligands to produce nanoclusters, followed by a second reduction such that the nanoclusters assemble into a layered structure. We characterized the electronic, crystallographic, and optical properties of nacre-like structures.

KİRAL VE ÇOKLU LİGANDLA STABİLİZE EDİLMİŞ NANOKÜMELERİN VE SEDEF BENZERİ YAPININ SENTEZİ VE KARAKTERİZASYONU

Zekiye Pelin Güven

MAT, Master of Science Thesis, 2014

Tez Danışmanı: Yrd. Doç. Özge Akbulut

Anahtar kelimeler: Gümüş Nanoküme, Kiralite, Çoklu Ligand, Sedef

Özet

Biyosensör, biyoişaretleme ve optik alanlarındaki olası kullanımlarından dolayı nanokümeler son zamanlarda oldukça dikkat çekiyor. Bu tezde birden fazla çeşitli ligandla kiral özellik gösteren gümüş nanokümelerin sentezini ve karakterizasyonunu raporlayacağız. Nanokümelerin kiral özellikleri; farklı ligandlar kullanılarak, ligandlar arası oranlar ve toplam ligandın gümüşe olan oranı değiştirilerek araştırılmıştır.

Sedef benzeri yapılar seramik yapılardan daha fazla olan sertlik özelliğiyle çok sayıda araştırmaya konu oluyorlar. Bu sertlik sedefteki tabakaların organik biyomoleküller tarafından bir arada tutulduğu kompozit yapıdan gelmektedir. Bu yapı sayesinde uygulanan baskı yüzünden kırılmalar çok zorlaşmışır ve oluşan çatlakların ilerlemesi engellenmiştir. Sedef yapılı malzemeleri üretmek için organik ve inorganik katmanlar birbirleri üzerinde tek tek kaplama halinde birleştirilmektedir ya da organik matriksin içinde inogranik kısım in situ mineralleştirilmektedir. Bu tezde sedef gibi yapılar, gümüş nanoyapıların ikinci bir defa indirgenerek oluşturduğu nano/mezo büyüklüklerindeki yapıtaşlarının kontrollü bir biçimde katmanlı hale getirilmesiyle sentezlenecektir. Oluşan yapıların optik, elektronik ve kristalografik karakterizasyonu anlatılacaktır.

ACKNOWLEDGEMENT

My parents, Mahmut Nedim Güven and Meliha Güven for raising me with a sense of humor, supporting me, loving me, appreciating me.

My grandparents, Zekiye Arslan and Hüseyin Arslan, for their unending support and love.

My great little sister, Selin Güven and my dearest friend Gamze Pirinç for their love, support, and making my last two years in İstanbul more valueable.

Since I have been in Sabancı University for 7 years, I would like to thank to my dear friends Naz Doğan, Aydın Özcan, Kayahan Sarıtaş, Doğa Gizem Kısa, Barış Dinçer, Sami Sarper Yazıcılaroğlu, Berfin Canpolat and Nilay Er for their encouragements, friendliness and making my time worthful in SU.

TABLE OF CONTENTS

LIST OF FIGURES

LIST OF SYMBOLS AND ABBREVIATIONS

LSPR	Localized Surface Plasmon Resonance
PAGE	Polyacrylamide Gel Electrophoresis
TEMED	Tetramethylethylenediamine
IBAN	Intensely and broadly absorbed particles
UV	Ultra Violet
ORD	Optical Rotatory Dispersion
PMT	Photo Multiplier Tube
CD	Circular Dichroism
L-cys	L-cysteine
MHA	Mercaptohexanoic acid
D-cys	D-cysteine
mM	Milimolar
MBA	Mercaptobenzoic acid
MPAA	Mercaptophenylacetic acid
MP	Mercaptophenol
RT	Room temperature
ME	Mercaptoethanol
TEM	Transmission Electron Microscopy
SEM	Scanning Electron Microscopy
XRD	X-ray Diffraction
θ	Theta
nm	Nanometer
°C	Degree Celsius
SAXS	Small Angle X-ray Scattering

To ones who support me no matter what; my beloved family and my heavenly grandparents...

CHAPTER 1

INTRODUCTION

1.1 Nanoclusters

Nanoclusters are groups of atoms that form structures generally smaller than 2 nm. The quantum size effects that nanoparticles do not have appear when the size of the structure gets down to this size scale [1]. For example, localized surface plasmon resonance (LSPR), which is a coherent oscillation of conduction band electrons influenced by incident electromagnetic radiation, changes drastically depending on the number of atoms in a structure, shape, and dielectric properties of a structure [2]. (Figure 1)
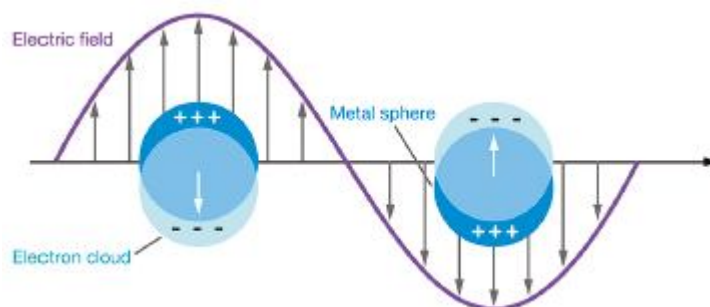
Figure 1: Schematic diagram that represents localized surface plasmon resonance, indicating oscillation of conduction electron cloud relative to nuclei [3]

Stability of synthesized structures, in other words prevention of aggregation is crucial to control these properties. There are two ways to stabilize ; electrostatic stabilization and steric stabilization [4]. When ions are absorbed on the surface of metal structure, the electrostatic stabilization occurs. Due to this charged layer, Coulombic repulsion force

between each nanocluster keeps them separated. If the adsorbates on the surface are polymers or bulky ligands, nanoclusters can stay separate due to steric stabilization.

There are several ways to synthesize nanoclusters including electrochemical synthesis, transition metal salt reduction, metal vapor synthesis, thermal decomposition, and photochemical methods [4, 5]. Optical and electrical properties of nanoclusters, due to their small size, strongly depend on their structural properties such as size, shape, and monodispersity in synthesis [6]. Similar to nanoparticles, to utilize the full potential of this size scale, monodisperse populations should be realized. Separation techniques such polyacrylamide gel electrophoresis (PAGE), filtration, and chromatography are used to enrich monodisperse populations of nanoclusters.

1.1.1 Polyacrylamide Gel Electrophoresis

PAGE is one of the important separation methods for proteins and aminoacids in biotechnology. The polyacrylamide gel is the medium for separation under applied voltage. There are two parts that form the gel between glass slides: stacking and separating gel. Stacking gel contains the wells which are formed by inserting a comb before crosslinking; samples are loaded to these wells and they are stacked at the bottom of these wells by applied voltage. (Figure 2) Stacking gel has lower monomer ratio leading to formation of bigger pores. Therefore, all of the structures can propagate through this gel. Separation gel has smaller pores and this is the place where the separation occurs.

Polyacrylamide gels are formed by polymerization of acrylamide and bis-acrylamide (N ,N'-methylene-bis-acrylamide) which is initiated by ammonium persulfate and tetramethylethylenediamine (TEMED). TEMED also catalyzes the reaction by accelerating the formation of free radicals from persulfate which activates acrylamide monomers [7]. In this reaction, bis-acrylamide is used as a crosslinker. The ratio of monomer to crosslinker can be changed to tune pore size for separation of structures with different size.

While the porous structure of the gel provides the separation of structures in terms of size, applied voltage makes separation based on charge possible. Therefore, regarding

the characteristics of structures they can be separated according to their size, charge, or both.
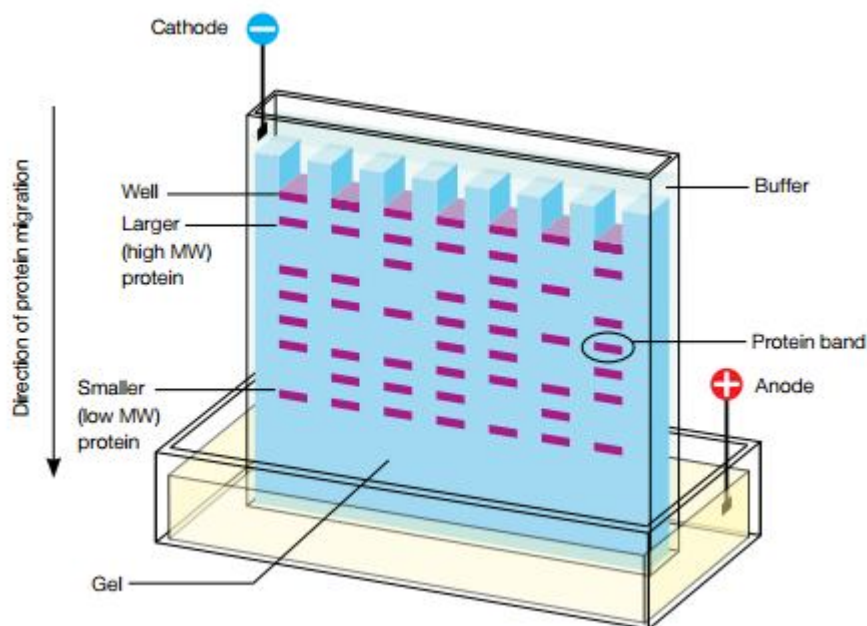
Figure 2: Schematic illustration of PAGE [8]

1.2 Magic Number Clusters

Nanoclusters can be classified by the amount of atoms they contain in the metal core. Some synthesis routes provide a dominance of metal cores with certain atom numbers [9]. These are the numbers of atoms make these cores have complete and regular outer geometry, in other words closing of atomic shells. These clusters, called magic number clusters, have more stability due to their full-shell geometries and densely packed arrangements which provide maximum amount of metal-metal interactions [10].

Bakr, *et al.* studied structure of $[Ag_{25}(SH_{18})]^-$, called intensely and broadly absorbed nanoparticles (IBAN) theoretically and experimentally [11]. Harkness, *et al.* investigated $Ag_{44}(SR_{30})^{4-}$ structures, called silver-thiolate superatom complex [12]. Yang reported structural analysis of $Au_{12}Ag_{32}(SR)^{30}$ inter-metallic compounds [13].

Full-Shell "Magic Number" Clusters					
Number of shells	1	2	3	4	5
Number of atoms in cluster	M_{13}	M_{55}	M_{147}	M_{309}	M_{561}
Percentage surface atoms	92%	76%	63%	52%	45%

Figure 3: Schematic illustration that shows the relationship between numbers of shells in a nanocluster and respective amount of atoms on the surface and in the cluster [14]

1.3 Mixed Ligand

The properties of nanoclusters can arise from interactions between the ligands that stabilize nanoclusters. For example, Janus particles have two distinct parts with different chemical and physical characteristics (hydrophilic-hydrophobic) leading to unique properties in terms of solubility and being pH responsive [15]. Apart from using a masking step in which a part of nanoparticles is made inaccessible to some reagents that a specific reaction occurs on other part, self-assembly of multiple ligands can be used to coat nanostructures [16]. To stabilize structures with several ligands, one-pot synthesis or ligand exchange reactions after synthesis can be used. Regarding characteristics of ligands and reaction conditions, arrangement of ligands on the particles can appear in several ways. (Figure 4)
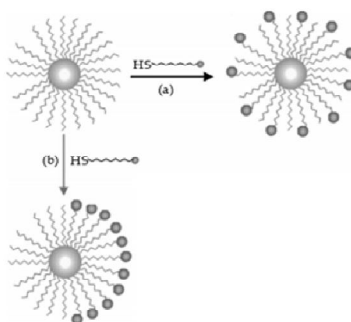
Figure 4: Schematic of surface functionalization based on ligand exchange reactions leading to a) bulk-exchange and b) Janus nanoparticles [17]

4

Carney *et al.* used combination of octanethiol (hydrophobic) and 11-mercaptoundecane sulfonate (hydrophilic) to synthesize amphiphilic gold nanoparticles and studied their interactions with lipid bilayers [18]. Catchart and Kitaev used captopril and glutathione to coat silver nanoclusters to investigate chiral properties [19]. Liu *et al.* used hexanethiol and mercaptohexyl naphthalenylmethyl thiol to make gold nanoparticles sensitive to polycyclic aromatic hydrocarbons [20].

1.4   Chirality

Chirality in chemistry is a geometrical term that is used to describe molecules that are not mirror images of each other. Use of this term for single molecules came out first by resolution of the structure of tartaric acid by Pasteur in 19th century [21]. The critical role of chiral molecules (e.g., DNA, proteins, and amino acids) has increased investigations in this field as well as on detection tools for the characterization of chirality. New synthesis and fabrication methods were devised to imitate naturally occurring chiral structures such as to produce chiral mesoporous silica [22], carbon nanotubes [23], and metal nanoparticles [24]. The novel optical properties of chiral structures make them potential candidates for sensing applications, since they are targeted towards chiral biomacromolecules.

Single molecules   Macromolecules   Living systems

Å nm   μm   mm

Individual chirality   Collective dissymetry
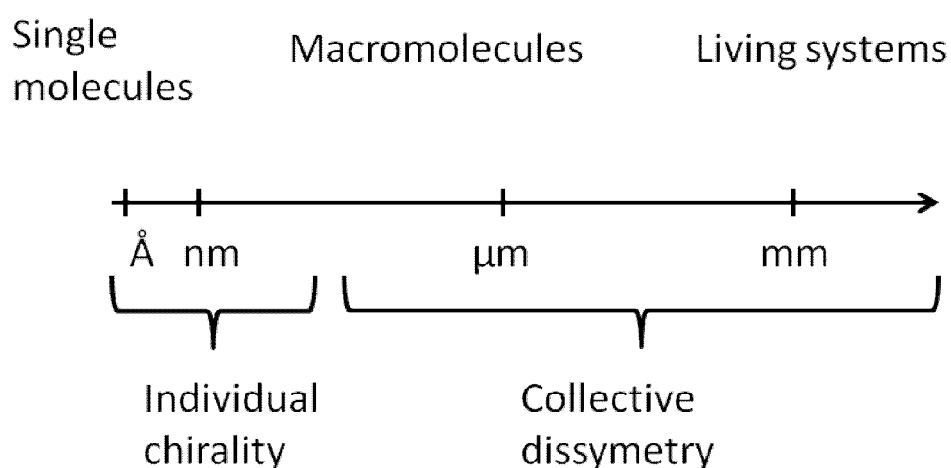
Figure 5: Size scale for types of chirality on molecules and living systems

Metallic nanoparticles have different optical properties than their bulk form due to the excitation of localized surface plasmon resonances. The combination of advanced

synthesis and surface modification routes of chiral nanoparticles, modifications in optical properties, and their possible enantiospecific interactions makes chiral nanoparticles gain further importance.

There are several ways to obtain chiral activity in nanoscale; intrinsic structure of particles or collective interactions between 3D ordered nanostructures can lead to chiral activity [25]. The causes of collective chirality can be summarized in three main classes: i) an achiral core can gain chirality via surface modification by chiral molecules, ii) existence of chiral ligands can affect the formation of chiral cores, and iii) chiral footprint can be formed in an originally achiral core by relaxation of surface atoms that adsorb chiral ligands (i.e., chiral footprint model) [26]. There are also exceptions which cannot conform one of these three classes such as dissymmetric field theory in which transmission through space acts as a perturbing field electrostatically to break down the symmetry of the electronic state of nanoclusters. Although it elucidates that chiral response of coated particles appears due to chiral centers on the ligands [26, 27], it does not provide the results for L-/D-penicilamine coated silver and gold nanoclusters with same size [28]. Also, after ligand exchange reaction on gold nanoclusters this theory does not explain the corresponding chiral response experimentally in which there was no change, although the calculations through it induce a change in chiral response [29, 30]. Additionally, chiral footprint model fails with the temperature dependent chiral response on gold nanoclusters [31]. In general, above-mentioned theories are used in combination to explain the chiral response of chiral nanostructures.

Imposing chirality in metal nanoparticles has not been advanced yet both theoretically and experimentally due to the difficulties in sustaining chiral properties when particles get bigger. Mostly the combination of achiral cores and chiral ligands provide the chiral activity [32]. However, in nanoclusters with a size of smaller than 2 nm, chirality can be referenced to all of the mechanisms that mentioned above. For nanoclusters, corresponding chiral responses are observed in UV region of the spectrum due to shift of surface plasmon resonance and they mostly have low chiral response. Chiral response has been acquired by several ways in silver nanoclusters; Cathcart *et al.* coated silver nanoclusters with two different chiral ligands [33], Nishida coated silver nanoclusters with L, D.penicilamine [28], Farrag, *et al.* coated silver nanoclusters with N-Acetyl-L-cysteine and L-glutathione [34], and Yao synthesized 3-Mercaptophenylboranic acid

coated silver clusters and with existence of L- and D-fructose these clusters induced chiral response [35].

While individual chirality is hard to obtain in metal nanoparticles, collective chirality occurred in assemblies with a covalent bond linkage of nanoparticles with different composition or a linkage of nanoparticles to a chiral template [25]. .

1.4.1   Circular Dichroism Spectroscopy

Optical active compounds contain chiral molecules and optical activity is a macroscopic property which arises from the way these molecules interact with light collectively. The incoming light is absorbed by the optically active molecules unequally that the combination of adsorbed lights leads to a measurable difference. Characterization tools based on this principle are used to measure the chiral response of structures such as circular dichroism spectroscopy, fluorescence detected circular dichroism spectroscopy, vibrational circular dichroism spectroscopy, raman chiral response, and optical rotatory dispersion (ORD) measurements. ORD depends on the dispersion of linearly polarized light leading to an optical rotation of the light at the end. (Figure 6) Excluding ORD, most of these methods are based on the principles of circular dichroism. It is the difference between absorption of left and right circularly polarized light at some wavelengths by optically active structure due to difference in molar extinction coefficients for the two polarized lights. (Figure 6) In other words, circular birefringence of chiral molecules leads to an anisotropic medium in which left and right circularly polarized waves propagate at different speeds.
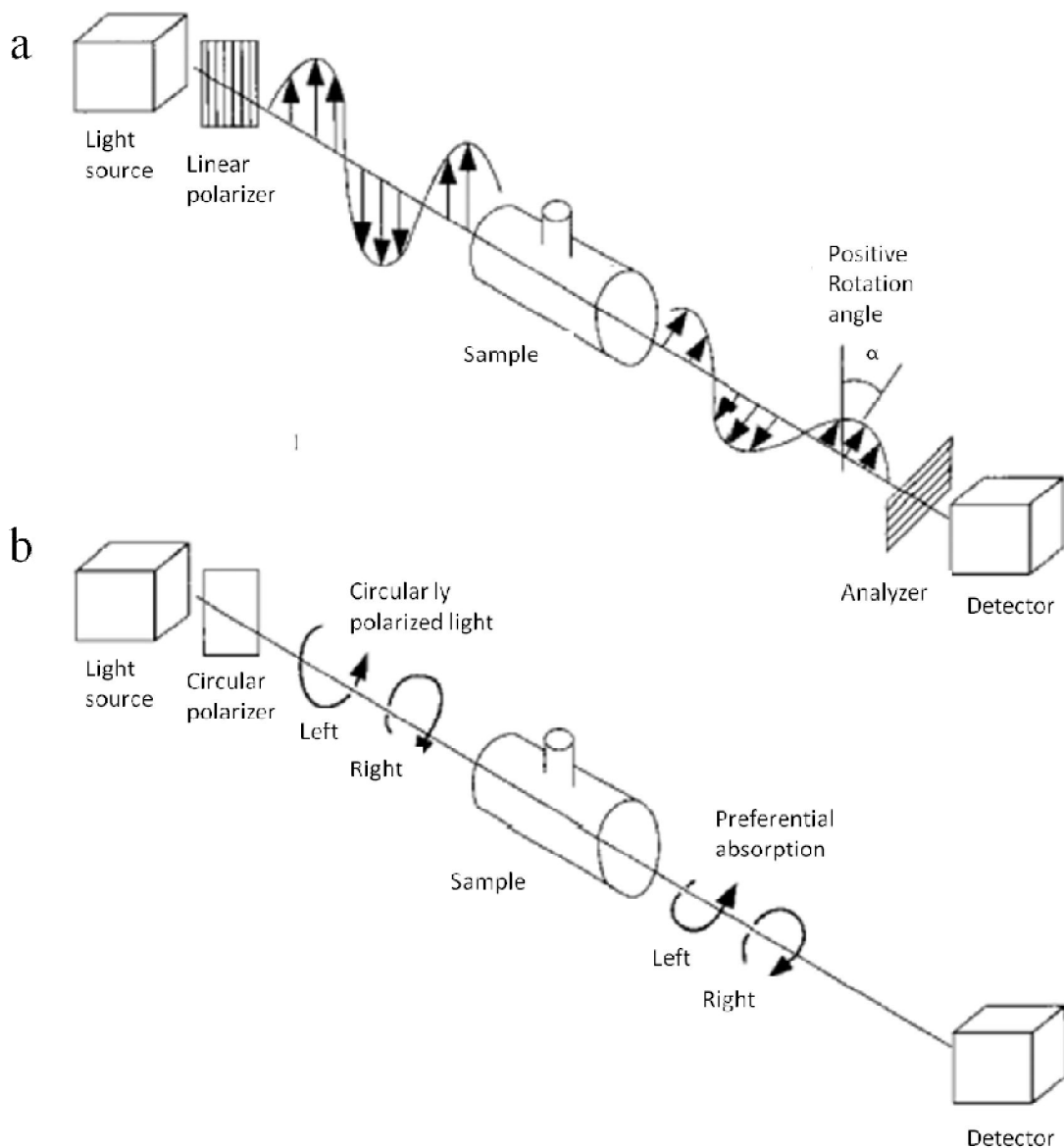
Figure 6: a) Schematic illustration of rotation of linearly polarized light, b) circular dichroism [36]

When the left and right circularly polarized lights are absorbed by different amounts, circularly polarized light is converted to elliptically polarized light. This light is detected by a photo multiplier tube (PMT) and converted into circular dichroism (CD) signal. This phenomenon is mainly used to investigate secondary structures of polypeptides.
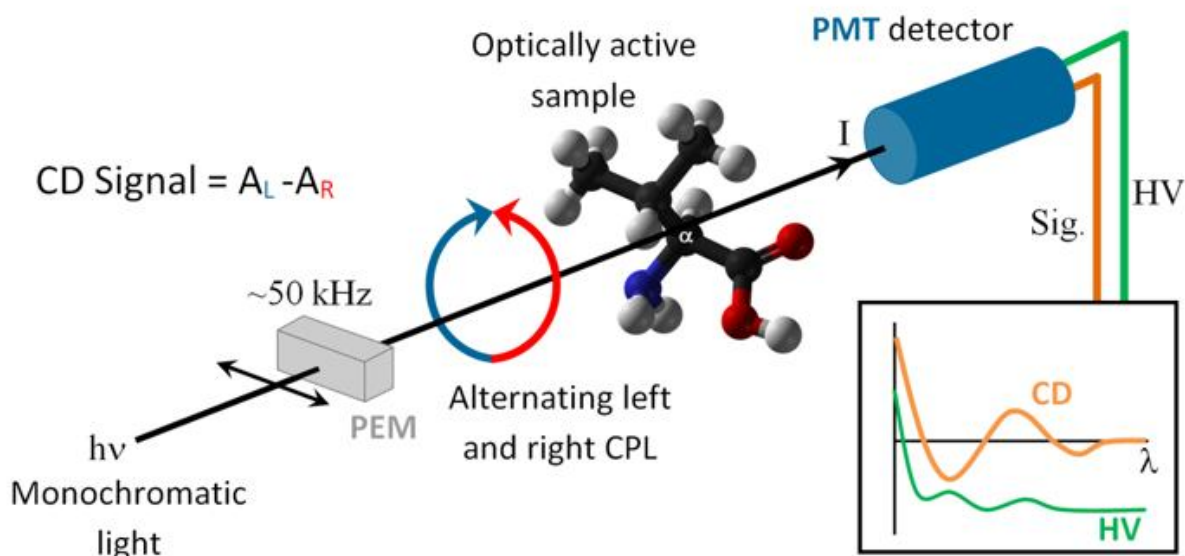
Figure 7: Schematic illustration that demonstrates working principle of circular dichroism spectroscopy [37]

The unit of the circular dichroism is ellipticity which is the ratio of minor to major elliptical axis. It is represented in millidegrees, such as the ratio of 1:100 corresponds to ellipticity of 0.57 degrees. Most of the time for reasonable comparison of circular dichroism molar ellipticity is used;

$$[\theta] = \theta / (10 \times c \times l)$$

where c is the molar concentration of the sample (mole/L) and l is the path length (cm).

Optical rotation occurs as a result of difference between refractive indexes that leads to rotation of the plane of linearly-polarized light. This rotation is due to difference between speeds of electric components of the wavelength that propagates in optically active structure. Since both ORD and CD are wavelength responsive, they can be calculated from each other. The relationship between the absorption and rotation is called Cotton effect [38]. Figure 8 indicates that when ORD starts to increase after the wavelength at which CD response is maximum, it is called positive Cotton effect. Otherwise it is negative.
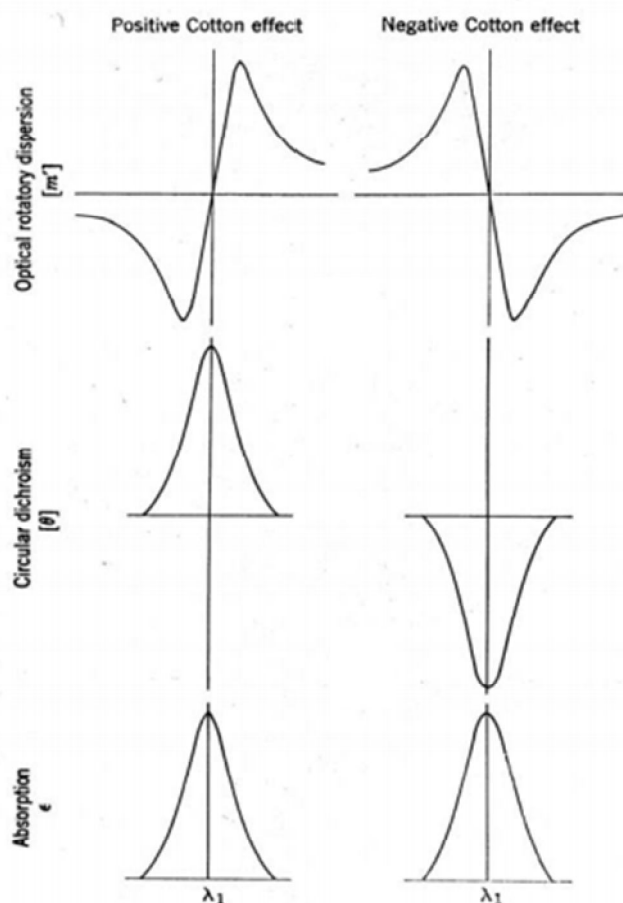
Figure 8: The relationship between optical rotatory dispersion, circular dichroism spectra, and absorption in terms of Cotton effect [38]

This scheme shows the correlation between absorption of the chiral structure and its circular dichroism. Absorption and chiral response can appear at the same wavelength. This relationship points the role of metal cores in chiral response.

Although ligands themselves show chiral response in the UV region, their interaction with nanoclusters leads to chiral responses in the visible region. Experimental work is supported by computational research to explain these phenomena. Schaaf-Wheten and Yao first showed the mirror image of chiral response in clusters by coating gold clusters with enantiomers of penicillamine [27, 39]. Yao compared the conformational effect and vicinal effect of chiral response on clusters. The large chiral response of nanoclusters is explained by this effect. The chiral response increases with a decrease in size of the nanoclusters due to higher surface-to volume ratio of smaller nanoclusters

and larger affect of chiral ligands on metal core parts of clusters by higher dissymmetric field [40].

1.4.2 Theories for Calculating Circular Dichroism Response

In circular dichroism measurements, wavelengths of chiral responses can be calculated. Different models are taken into consideration regarding optically active molecules. For clusters, the amounts of atoms are enough to use first principle calculations (e.g., coupled-dipole approximation). Coupled-dipole approximation is used to investigate the CD of chiral clusters for the first time by Roman-Velazquez [41]. In this theory, each atom is considered as an electric dipole with an isotropic polarizability. For this approximation there are two requirements; i) particles should be smaller than wavelength of light and ii) the interparticle distance should be bigger than particle size. This model considers a set of dipoles which are arranged at specific locations in space. Their individual dipoles to incident light are contributed by electromagnetically collective dipoles regarding scattering fields, leading the base for this assumption. For the bigger nanoparticles exciton-coupling theory can be considered in which scattering of light by particles dominates the chiral response [42].

Silver displays better optical properties than gold, but the stability of gold is better. The chiral response of silver is speculated to arise from easily oxidizable nature of silver which leads to a better interaction with ligands and consequently a larger distortion of symmetry due to adsorption [43].

CHAPTER 2

SYNTHESIS AND CHARACTERIZATION OF MIXED LIGAND SILVER NANOCLUSTERS

In this thesis, we show the synthesis and characterization of chiral nanoclusters that are stabilized in a mixed ligand system. We explored the matrix of conditions that leads to the formation of clusters. L-cysteine (L-cys) is a chiral ligand that has not been employed in the synthesis of chiral nanoclusters; we claim that the existence of mercaptohexanoic acid (MHA) is critical in the formation of clusters and L-cys, in the presence of MHA, imports chirality to these structures.

2.1   Optical Properties

Spherical silver nanoparticles absorb visible light ~400 nm leading a yellow-brownish color [44]. Due to their smaller size, clusters can lose their particle-related properties (e.g., continuous band absorptions) [45] and gain new ones regarding their molecular state (e.g., state filling and excited state absorptions) [46].

The product that we obtained from L-cys:MHA ratio of 1 to 1 is red/pink in color. (Figure 9) The peaks which appear at around 385 and 550 nm indicate the formation of clusters [47]. (Figure 10) Nanoparticles have red or blue shifts in their LSPR depending on increase and decrease in particle size, respectively, due to Mie theory. However, for clusters (<2 nm) even drastic shifts and appearances in LSPR have been observed (e.g., IBANs) [11], wavelengths of the absorbance do not correspond to the size of clusters [48]. On the other hand, surface plasmonic transitions are broader and have lower intensity for smaller clusters due additional scattering processes of the oscillating electrons at the surface [34]. The peak below 400 nm is attributed to electronic

interaction of metal core and ligands [48] and the peak at 550 nm is claimed to be due to large HOMO-LUMO gap associated with discrete energy levels [47].

Figure 9: As-synthesized mixed ligand silver nanoclusters
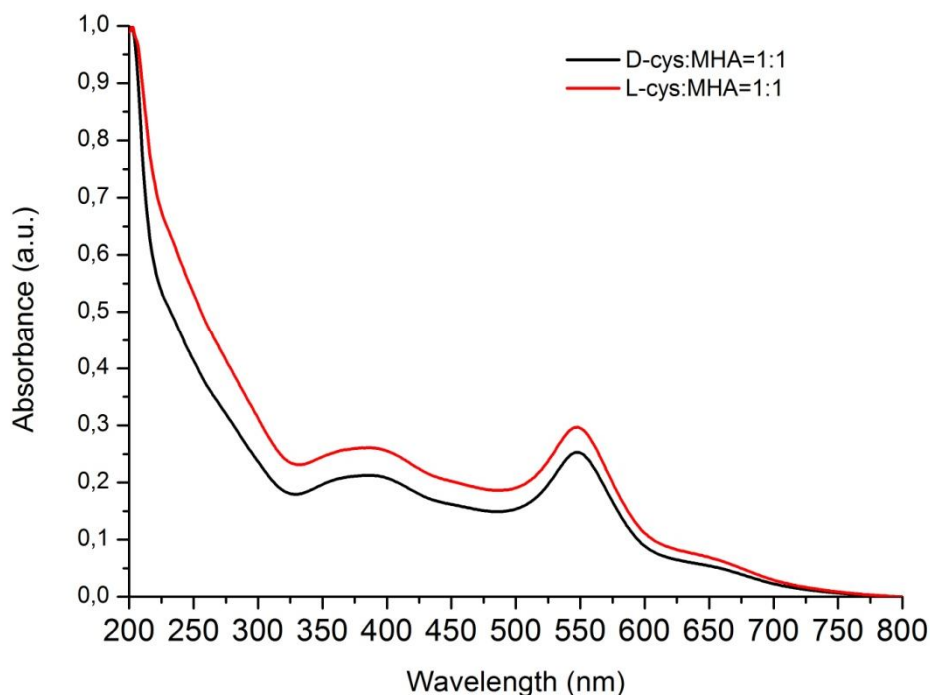
Figure 10: UV-vis spectra of clusters with different enantiomers

To monitor chiroptical response of the clusters, we carried out CD measurements. CD spectrum of 1 mM aqueous solution of pure L-cys is shown in Figure 11. The only significant peak on this spectrum is below 200 nm. On the other hand, nanoclusters with

mixed ligands induce chiral response at several wavelengths such as ~ 210, 275, 310, and 350 nm. (Figure 11) The difference between these two spectra complies with the theory of chirality based on metal-ligand interaction. Although the yields of formation of cluster with each enantiomer differ slightly, the normalized amplitudes of chiroptical responses resulting from clusters are almost the same. While nanoclusters with D-cysteine (D-cys) provide a positive response, ones with L-cys lead to opposite. This result contributes to the idea of chiral ligand-metal interaction based chirality on the nanoclusters.
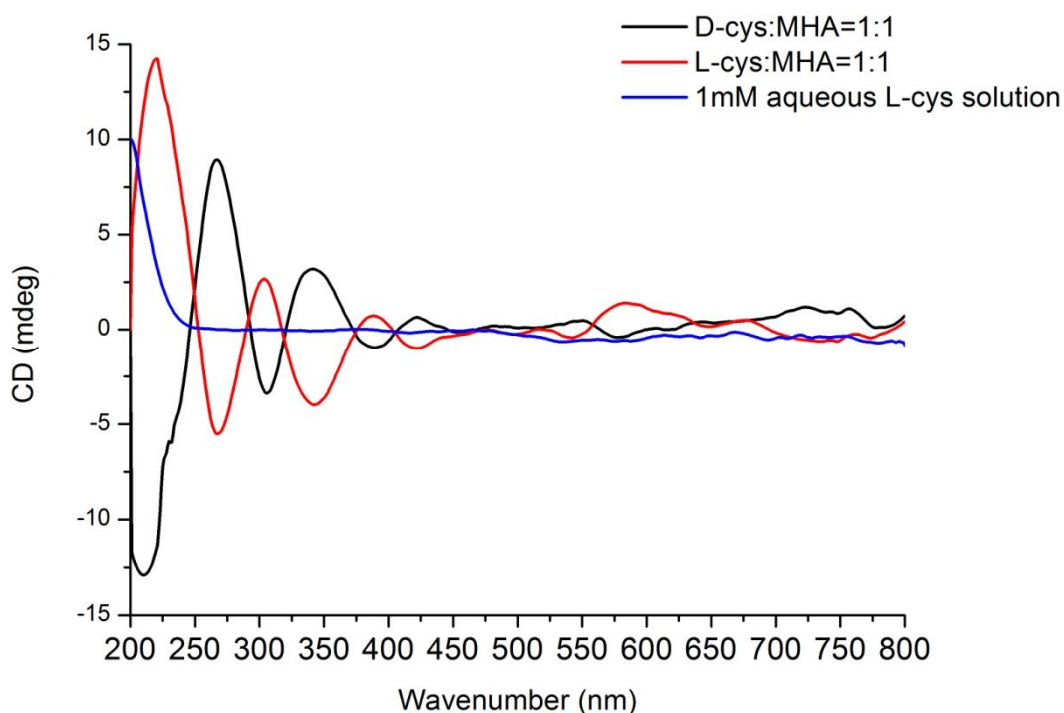
Figure 11: CD spectra of clusters with different enantiomers and 1 mM of aqueous L-cys solution
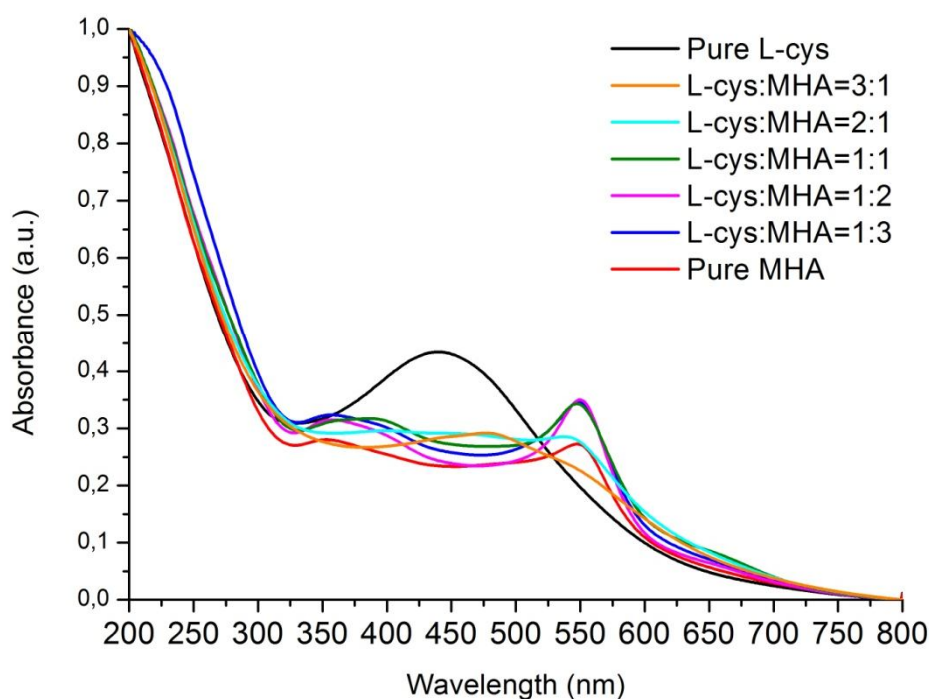
Figure 12: UV-vis spectra of the structures with different ligand ratios (L-cys:MHA)

We systematically changed ligand ratio to determine the matrix of conditions that produce clusters. We kept silver to thiol ratio constant (1:1) while changing the ratio of ligands (L-cys:MHA) among themselves. We obtained the most pronounced peaks from samples with ligand ratios of 1:1 and 1:2. The use of solely L-cys resulted in the formation of silver nanoparticles that revealed a characteristic peak at 440 nm due to surface plasmon resonance of these nanoparticles. (Figure 12) Although all of the samples were reddish after 6 hours, during the measurements the ones with more L-cys were more likely to lose that red color and turn into brown. In other words, the more L-cys the samples have, the more likely they got oxidized or aggregated.

We monitored the chirality of these clusters via CD spectroscopy. Again, the clusters with ligand ratios (L-cys:MHA) 1:1 and 1:2 demonstrated slightly larger CD peaks. We also observed a subtle shift to higher frequencies with increasing amounts of MHA. (Figure 13)
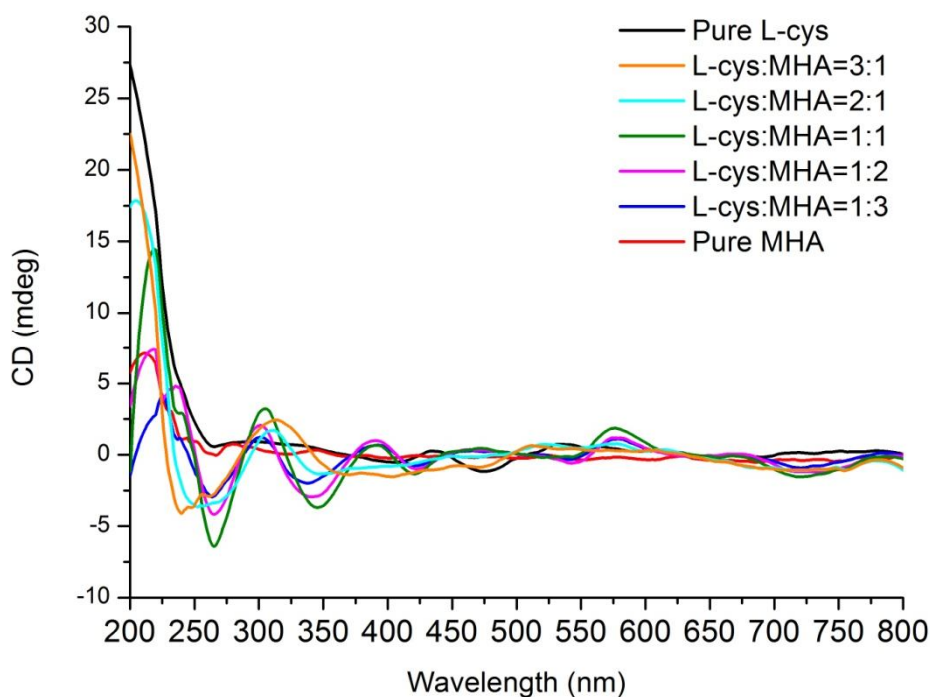
Figure 13: CD spectra of clusters with different ligand ratios (L-cys:MHA)

We carried out PAGE on the as-synthesized clusters since these systems were not monodisperse in size. (Figure 14) We further characterized the fractions of structures with L-cys:MHA ratio of 1:1 since this sample possessed the most pronounced UV-vis and CD peaks. (Number 4 in Figure 14) Only band number 4 from PAGE, exhibited the formation of nanoclusters as indicated by the double peak in UV-vis spectroscopy, and CD spectroscopy. (Figure 15 and Figure 16)
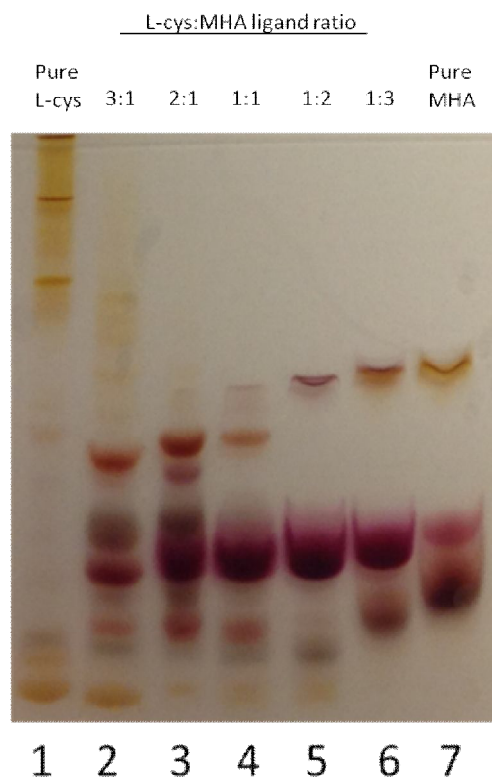
Figure 14: PAGE of the as-synthesized structures with different ligand ratio
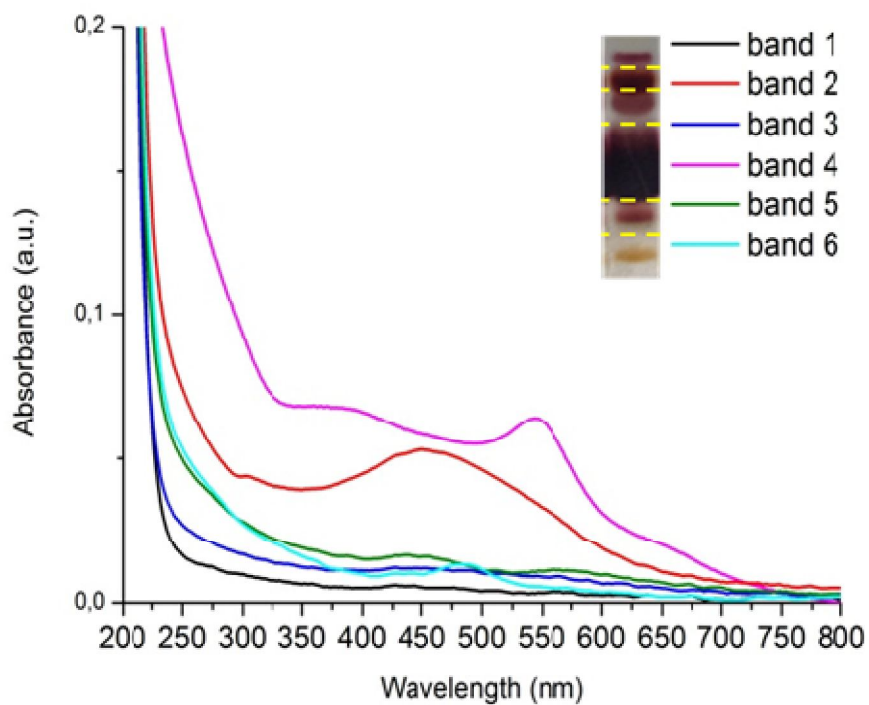
Figure 15: UV-vis spectra of fractions from PAGE of the sample with L-cys: MHA ratio of 1 to 1
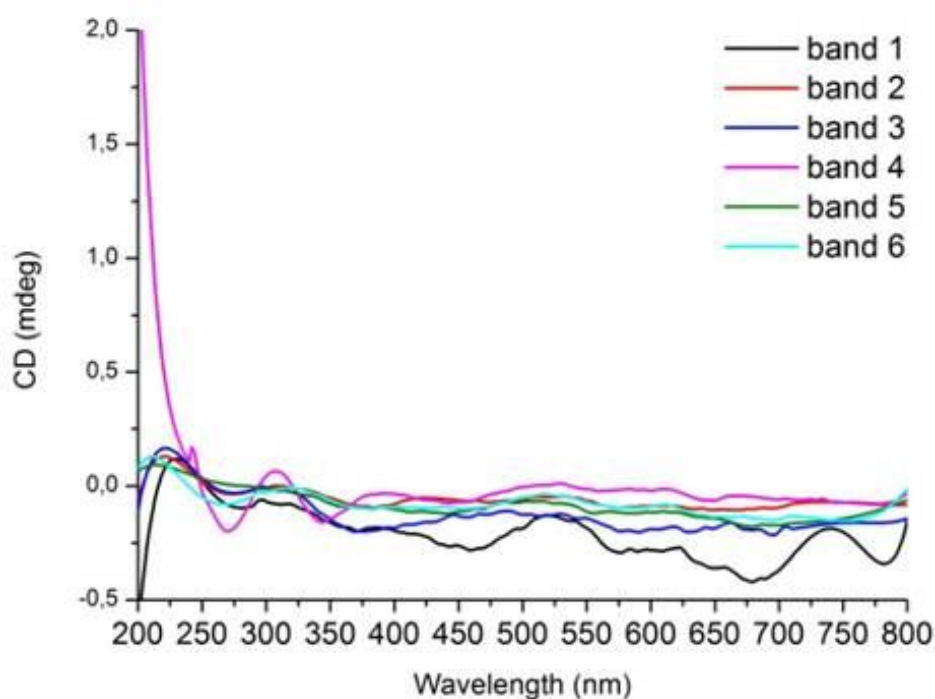
Figure 16: CD spectra of the fractions from PAGE of the sample with L-cys: MHA ratio of 1 to 1

In nanostructure synthesis ligand to metal ratio might affect the size of clusters [49]. Therefore, we tracked the silver to thiol ratios of these clusters at equimolar contributions from L-cys and MHA. The thiol amount in these experiments represents the total amount of L-cys and MHA. We observed the formation of clusters at ratios of 1:1, 1:1.25, and 1:1.5. However, at the ratio of 1:2 only a small amount of clusters was formed; yet all of these samples produced chiral signals in CD spectroscopy (Figure 17 and Figure 18).
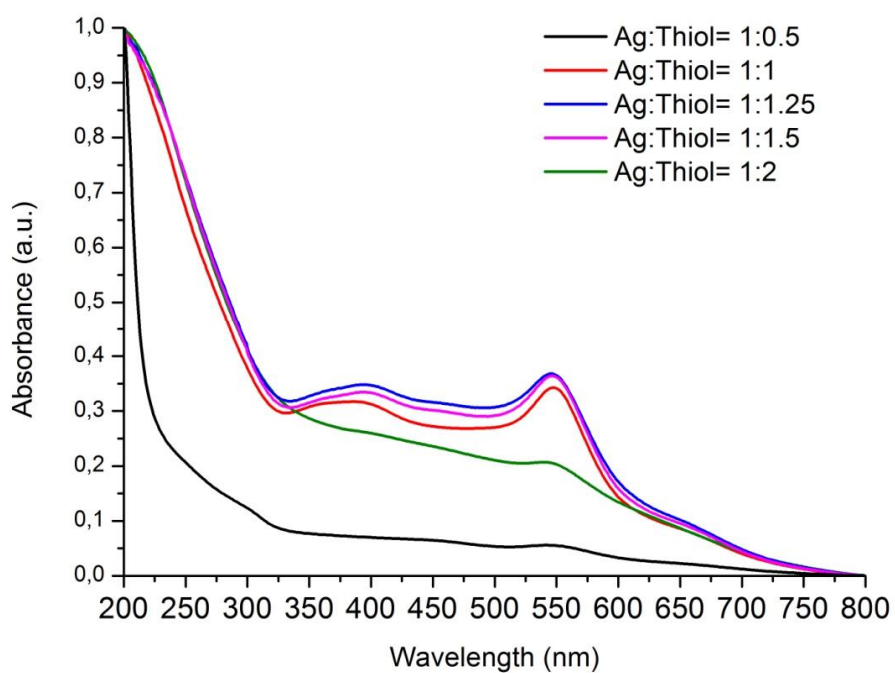
Figure 17: The UV-vis spectra of the nanoclusters that are synthesized with different silver to thiol ratios
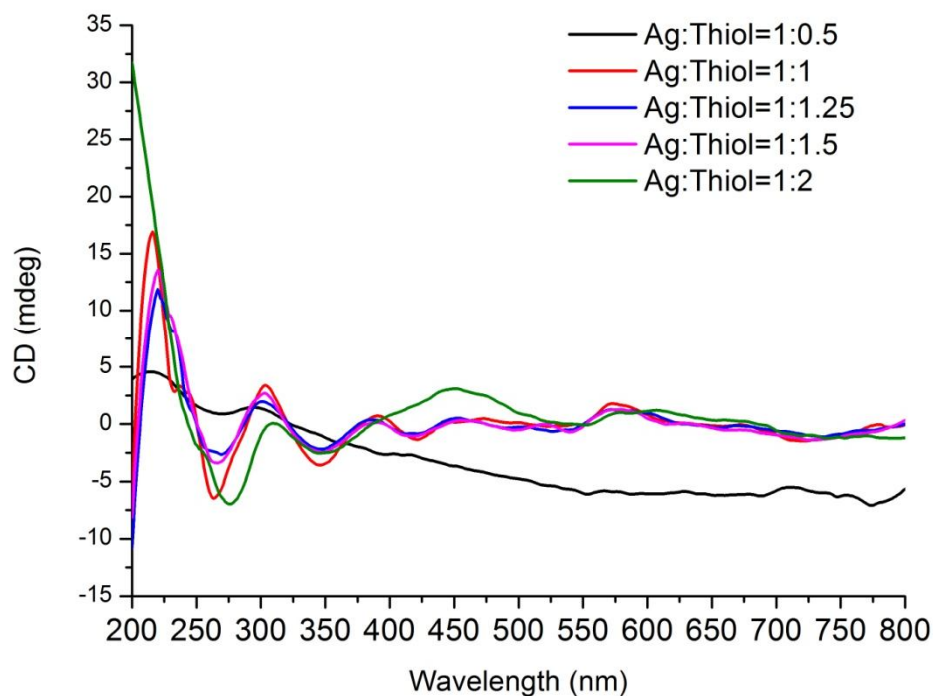
Figure 18: CD spectroscopy of reaction products with different silver to thiol ratio

In order to investigate the role of ligand combinations on the optical properties of nanoclusters, we used 3 different ligands instead of MHA in synthesis. Since we want our structures to have chiral response, we only changed the nonchiral ligand. We used mercaptobenzoic acid (MBA), mercaptophenylacetic acid (MPAA), and mercaptophenol (MP) to combine with L-cys at ratio of 1 to 1 which was optimized in Cys:MHA system. Although there was a subtle peak around 550 nm for the structures with L-cys:MPAA ligands, UV-vis spectra of structures contained peaks that were related to surface plasmon resonance of silver nanoparticles. (Figure 19) Additionally, CD spectra of these structures revealed no chiral structures. (Figure 20) To conclude, combination of Cys and MHA provides the best result in terms of chiral response.
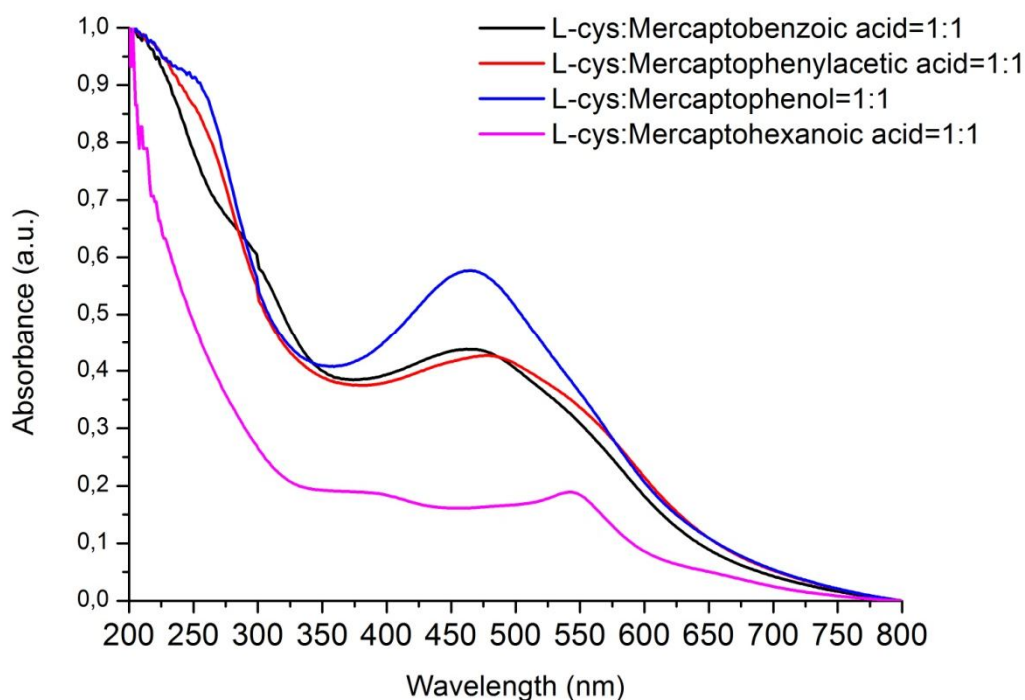
Figure 19: Effect of different ligands on the formation of nanoclusters
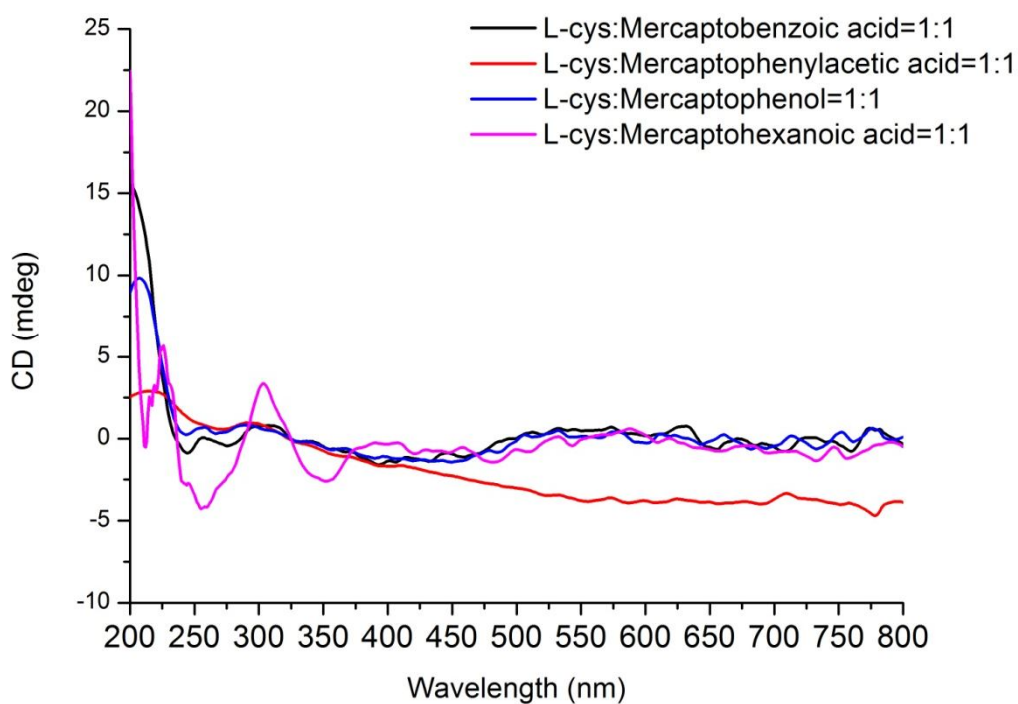
Figure 20: Effect of different ligands acid on chirchiral response

2.2 Stability

During synthesis, the formation of red/pink nanoclusters starts after an hour and we stop the reaction after 6 hours. If the clusters are left at room temperature (RT) in the reaction mixture, they aggregate irreversibly. To examine the effect of temperature and solvent on the stability of the clusters, we kept the clusters in i) their initial reaction environment (water/methanol solution at a pH of 11), ii) water/methanol solution, and iii) water. We also stored these solutions at -18°C, 4°C, and RT.

We observed a color change in the samples that are kept at RT just after 4 days while the others preserved their color. To monitor long term stability, we performed UV-vis spectroscopy after 3 weeks. The absorption peaks of clusters at 550 nm were preserved in the samples that were kept at -18°C and 4°C in methanol/water solution and in the initial reaction environment. (Figure 21) The instability of nanoclusters at room temperature is probably due to tendency of silver for oxidation.
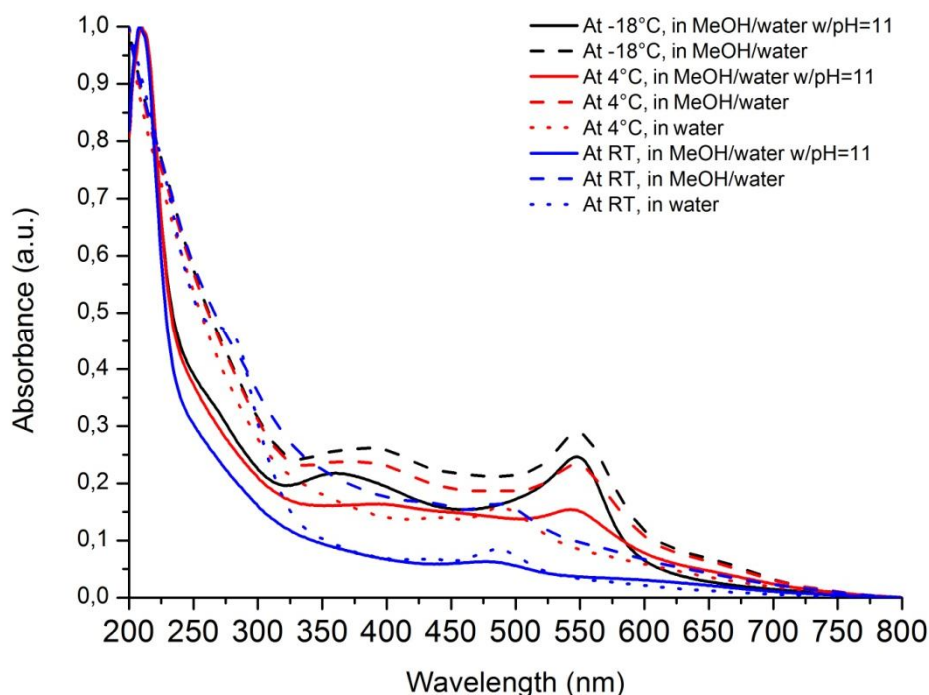
Figure 21: UV-vis spectra of samples with L-cys: MHA ratio of 1:1 that are kept at -18°C, 4°C, and RT in water, water/methanol solution and initial reaction conditions for 3 weeks

2.3 Particle Size

After extraction of clusters from PAGE to neutral distilled water, we realized that band number 4 in Figure 14 could preserve its red/pink color more than as-synthesized particles. (No data provided) We speculate that the reason behind was non-existence of extra ligands or chemicals that could lead oxidization or agglomeration of clusters. In other words, clusters are more stable after extraction than as-synthesized state. Since the reaction product was separated in PAGE, we had monodisperse clusters. To prepare samples for TEM, we drop cast some solution on the copper, Ted Pella grid and sucked the liquid with a Kimwipe laboratory cleaning tissue. Figure 22 indicates that there are some bigger structures in addition to nearly monodisperse nanoclusters with a size of ~3-4 nm. However, existence of some hollow shapes can be interpreted as polymer parts from PAGE extraction process.
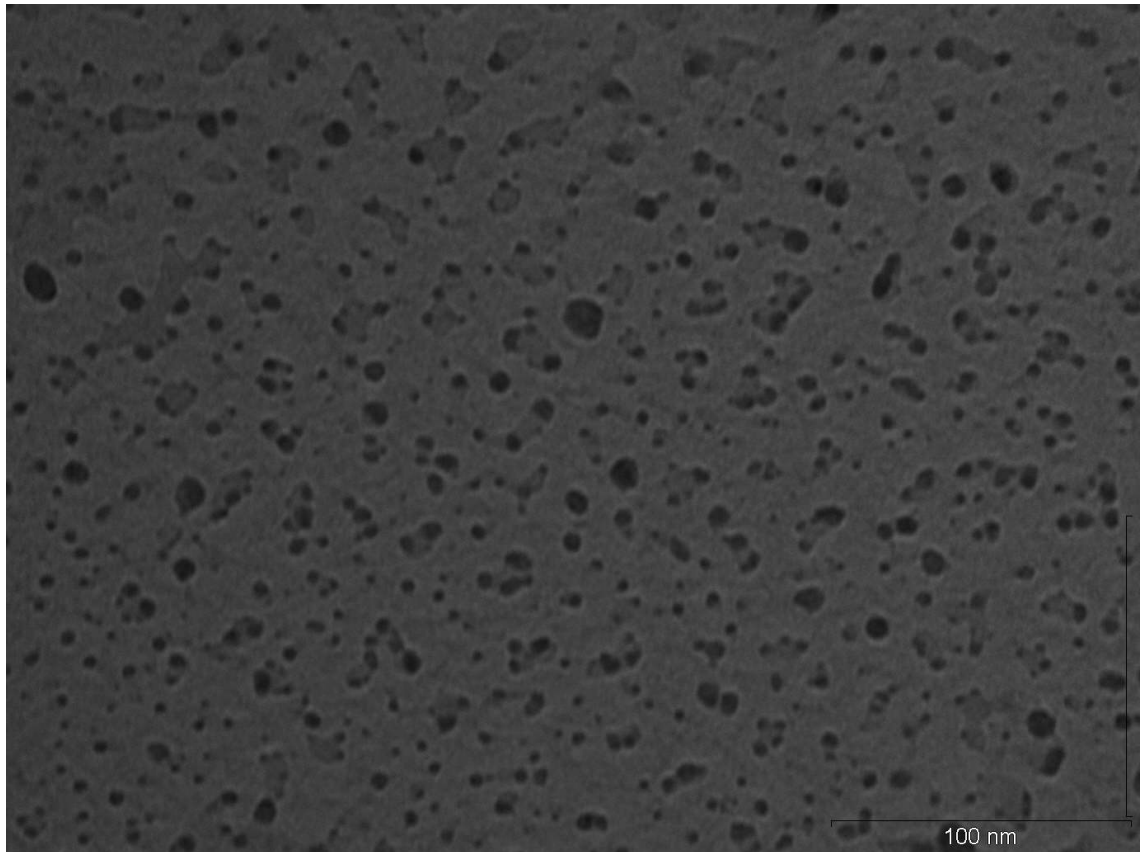
Figure 22: TEM image of nanoclusters that were extracted from PAGE

CHAPTER 3

SYNTHESIS AND CHARACTERIZATION OF NACRE-LIKE STRUCTURE

3.1 Introduction to Structure and Mechanical Properties of Nacre

Nature provides structures that engineers are keen on to replicate for the fabrication of leading airplane wings, self healing materials, and self cleaning polymers. Nacre has also gained attraction with its laminated composite structure [50] that leads unique combination of properties like hardness, toughness, and strength. Natural nacre (mother of pearl) has a brick-mortar type of structure (Figure 23) in which highly oriented ceramic aragonite structures form bricks and adhesive organic molecules form mortar.
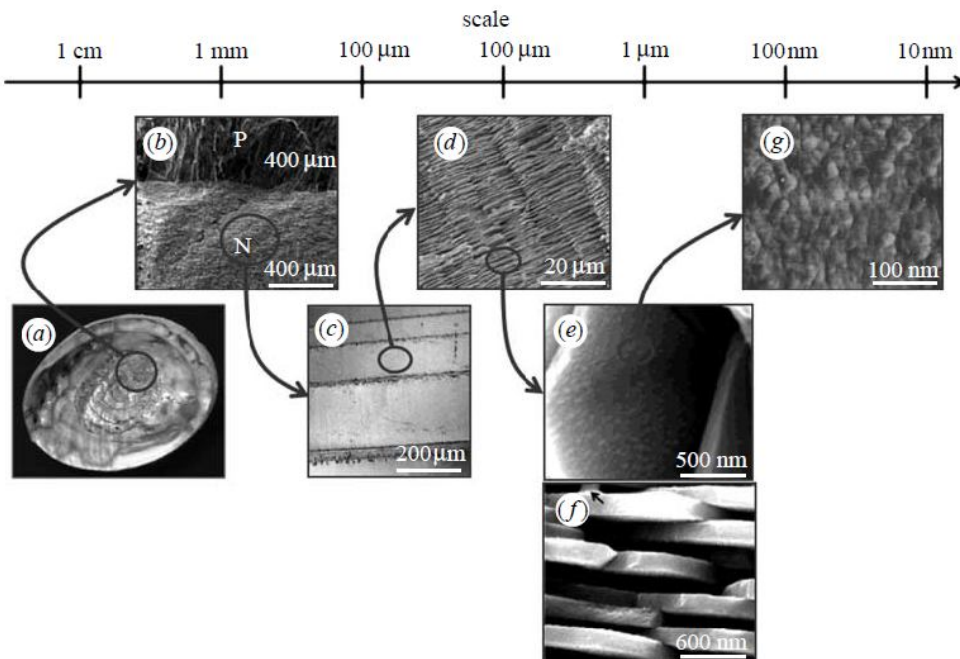
Figure 23: Hierarchical structure of nacre at seven different scales [51]

Composite structure of biomolecules (5% of the system) and platelets provide the unique properties of nacre by forming a mesoscale hierarchical arrangement. Existence of biomolecules prevents brittle aragonite platelets from crack propagation, while the nanoscale size of aragonite platelets ensures strength and maximum tolerance to flaws [52]. Additionally, biomolecules are elastic enough to make elongation possible in which platelets slide over each other even in millimeter scale [53]. Consequently properties such as ductility, resilience, and ability to dissipate energy are promoted [54, 55]. For example, the interdigitating structure of crystals and organic polymer matrix which directs the growth of crystals [56] yields fracture toughness approximately 5000 times larger than pure aragonite crystals [57]. There are also relatively recessive properties of nacre which advance the mechanical strength of nacre. For example, aragonite platelets contribute the mechanical strength of nacre mainly due to high orientation and lack of cleavage planes, although calcite structure is the most stable one among $CaCO_3$ structures [58]. Successive aragonite platelets have interlocks that contribute to the toughness of nacre via progressive fracture of interlocking [59]. Their waved surfaces also make sliding of platelets harder. Additionally the small asperities on aragonite platelets enhance shear strength of the structure [60]. Fraction of inorganic phase and degree of mineralization affects the mechanical properties of hybrid structure [61].

Although nature gives inspirations, the structures that can be synthesized have limitation, such as the tenacity at the interfaces and ability of self-repair in nacre structure [54]. Schaffer *et al.* showed that formation of nacre is not due to heteroepitaxial nucleation but growth through mineral bridges [62]. These mineral bridges form through the pores on interlamellar organic parts and decrease the weakness of interfaces in nacre structure by letting cracks to extend in them [17]. These architectural configuration and material characteristics of nacre are imitated to form new assemblies. While Oaki used K_2SO_4 as brick and polyacrylic acid as mortar to build a similar type of structure [63], Feng used Al_2O_3 aramid fiber and epoxy, respectively [56]. Tang combined clay and polymer to imitate the properties of nacre

[64], as Podsiadlo used starch stabilized silver nanoparticles with clay platelets to have antibacterial effect in biocompatible coatings [65].

3.2 Synthesis of Nacre Structure

We synthesized iridescent structure for the first time by addition of a second reducing agent, mercaptoethanol (ME) to already synthesized nanoclusters. (Figure 24) In the formation of nacre sample, the ligand ratios do not play a role and formation of nanoclusters is not required. When aggregated nanoclusters were reduced, the nacre structure was still formed. Additionally, existence of different ligands and type of silver precursor do not affect the formation of nacre, as well. Reduction of silver precursor by only ME in the presence of ligands leaded to nacre structure. In the other hand when we added ethanol instead of ME, there was no nacre formation.
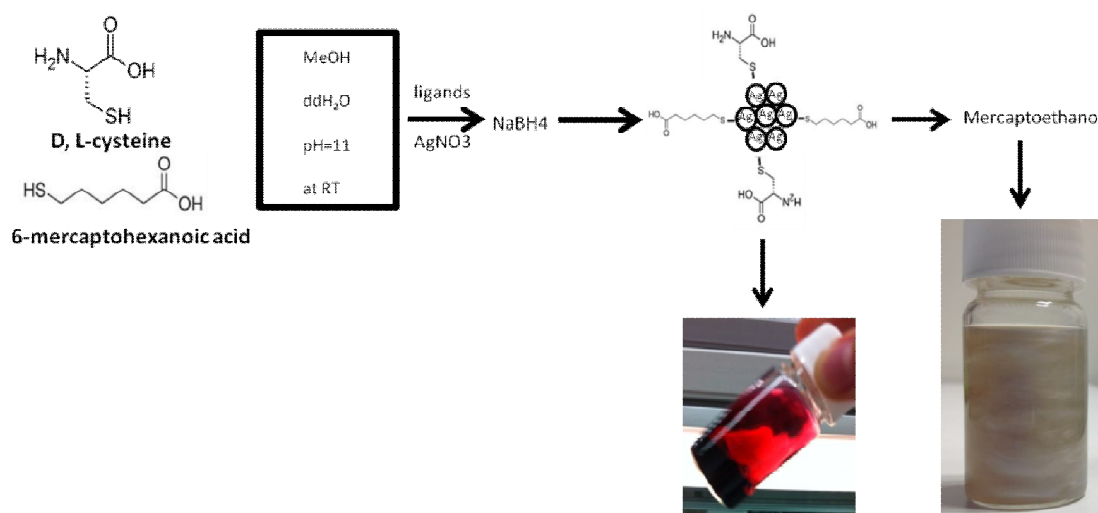
Figure 24: First synthesis route of iridescent structure

3.3 Characterization of Nacre Structures

We studied optical properties and structural properties of the nacre through XRD and electron microscopy, respectively.

3.3.1 Optical Properties

3.3.1.1 Effect of Ligand Ratio on Nacre Formation

To study optical properties of nacre-like structures, we used UV-vis and CD spectroscopy to examine the structure of nacre-like formation. In the absorption spectrum there is a distinct peak ~360 nm and there are small absorptions around 300 nm. (Figure 25) Although we started to synthesize these structures with 1:1 ligand ratio of L-cys:MHA, we checked different ratios for the formation of nacre. We started by using pure Cys in synthesis. By keeping the overall ligand to precursor ratio constant, we varied the relative ratios of ligands like (Cys:MHA) 1:3,1:2, 2:1, 3:1, and finally we eliminate Cys in the reaction. In each case we observed the prominent peak that we observed in samples with 1 to 1 ratio of L-cys:MHA. (Figure 25)
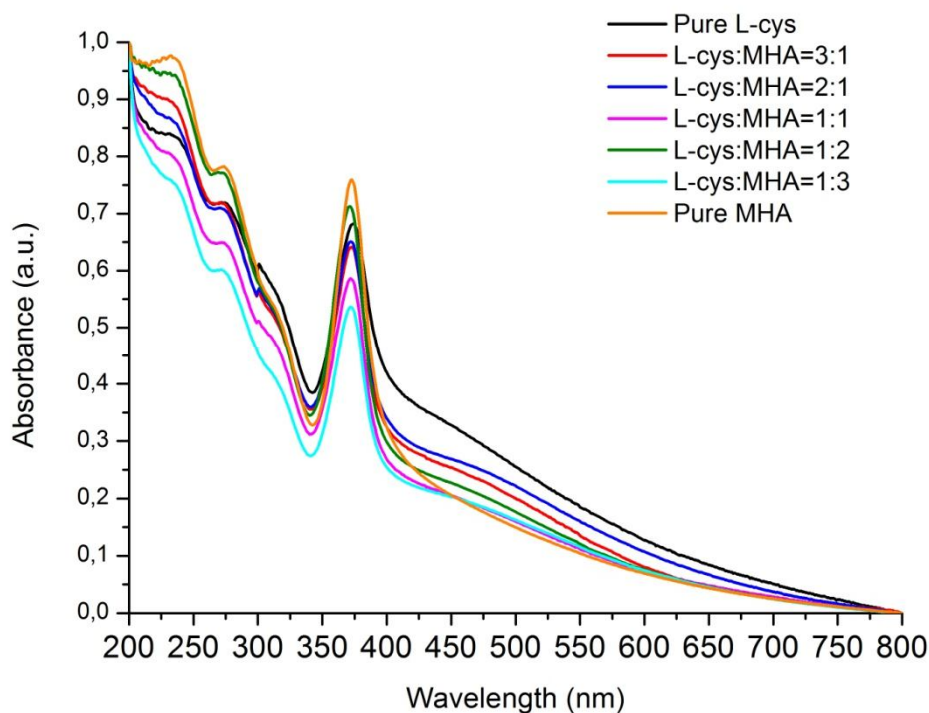
Figure 25: Effect of ligand ratio on the formation of nacre samples
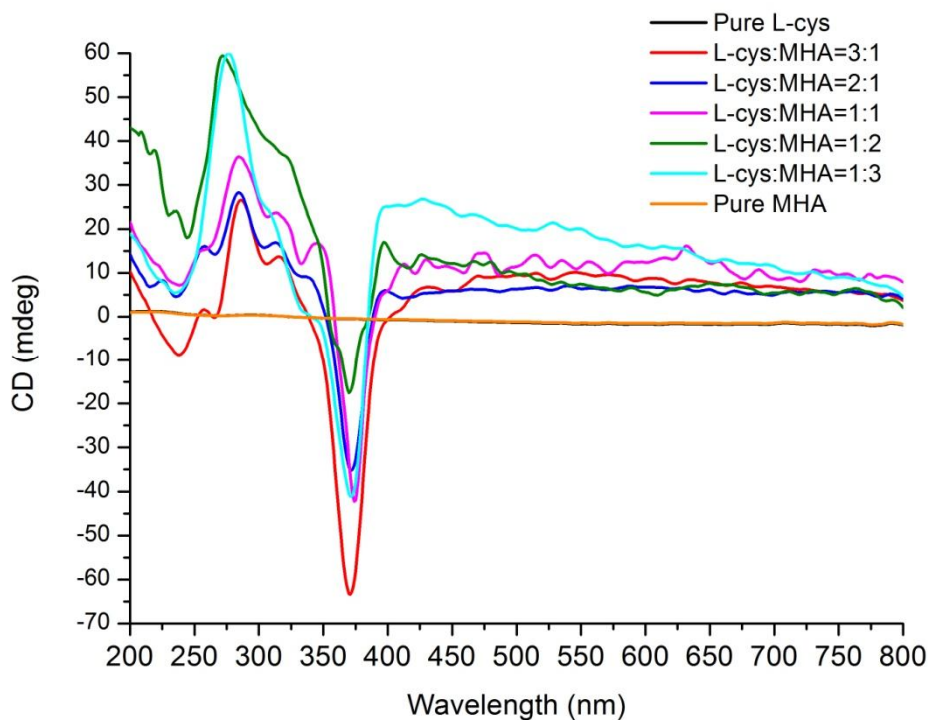
Figure 26: Effect of ligand ratio on the chiroptical properties of nacre samples (Spectrum for Pure L-cys i.e., black line is underneath of the spectrum for Pure MHA i.e., orange line.)

We characterized chiroptical properties for each samples with different ligand ratios. Figure 25 shows that combination of ligands lead to optically active structure, while structures with pure Cys and pure MHA were inactive. The wavelength that they induced chiral response (Figure 26) is consistent with the absorption that we monitored in UV-vis spectroscopy measurements. (Figure 25) To conclude, the structure that leads to absorption in near-UV also has the chiral response.

It was crucial to figure out whether this chiral response was due to small particles that are perfectly dissolved in reaction medium or the total solution of dispersed nacre-like structure. To understand this phenomenon, sample with L-cys:MHA ligand ratio 1:1 centrifuged three consecutive times at different conditions and each time the supernatants were undertaken to UV-vis and CD spectroscopy.
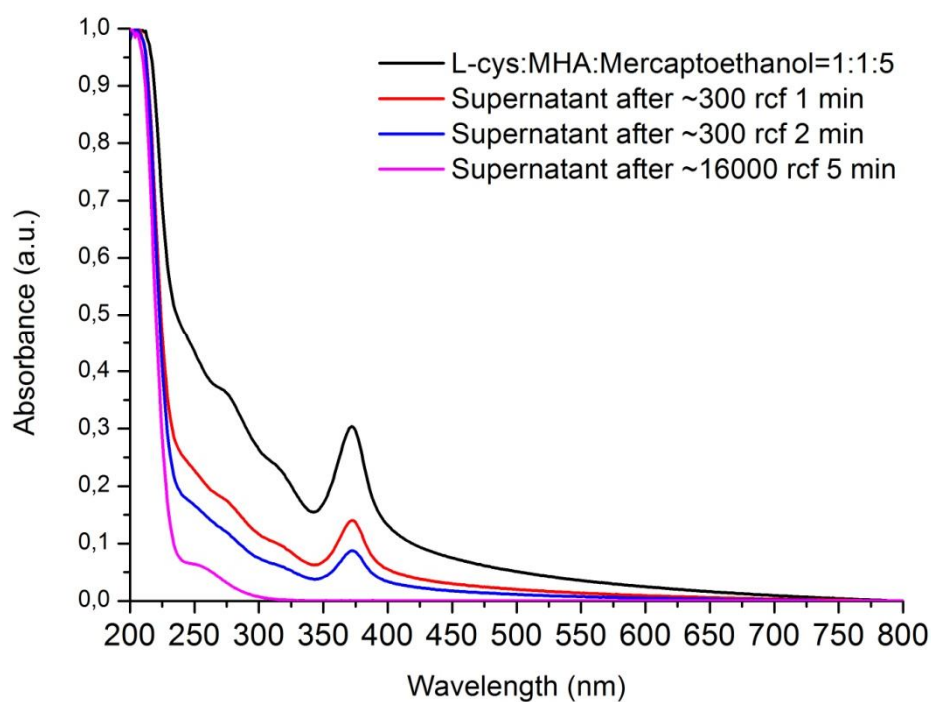
Figure 27: UV-vis spectroscopy on the supernatant after different amounts of centrifugation

This study proved that the chirality and prominent absorption peak were resulted from the dispersed nacre solution. Figure 27 and Figure 28 which induce that absorption and chiral response respectively were only monitored just after rotation at low rpm for a short time. In other words, peaks were provided by the dispersion of structures not the supernatant.
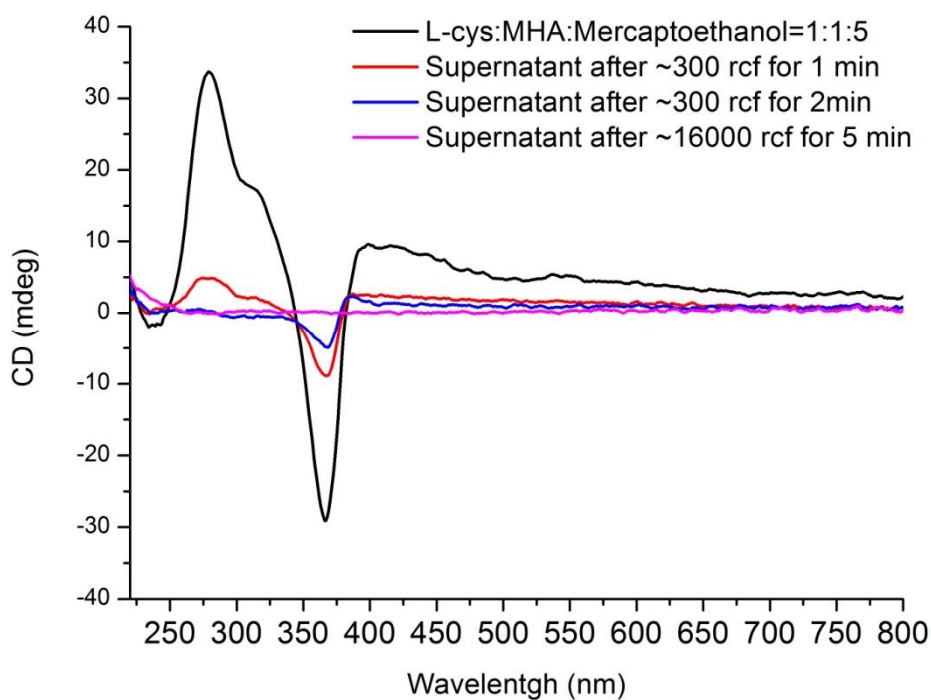
Figure 28: Effect of centrifuge on the existence of nacre sample in supernatant via CD measurement
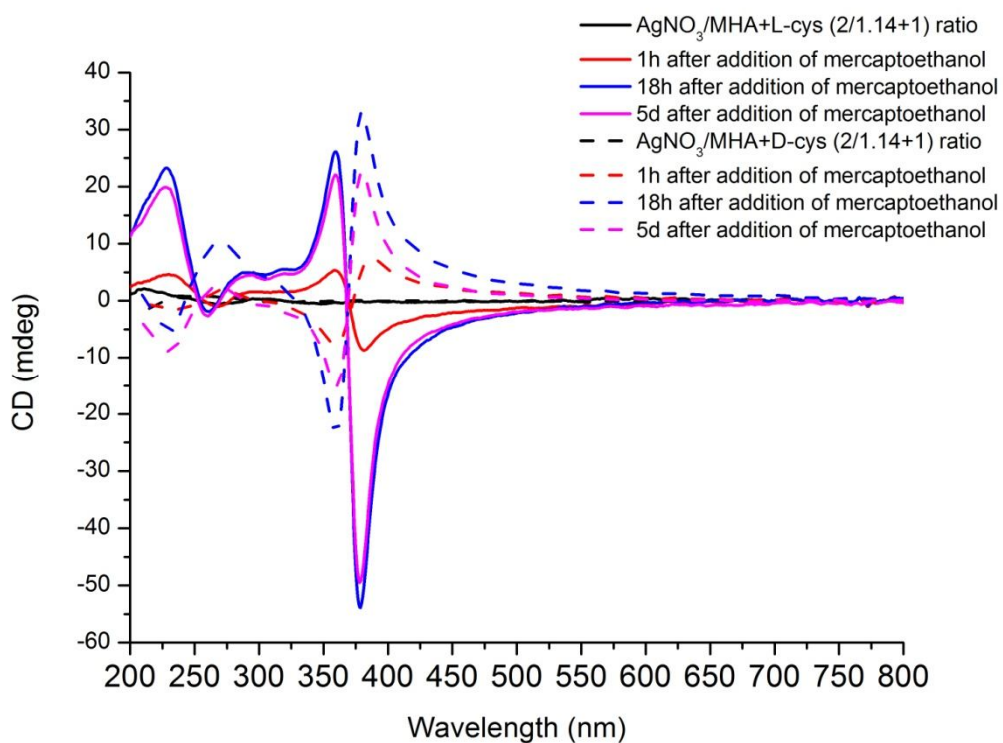
Figure 29: Enantiomer-based (L- and D-cys) chirality of nacre samples

Chiral response can depend on intrinsic chirality of metal cores or the chirality of ligands. To investigate the reason of chirality in our system, we used the enantiomer of L-cys and compare the samples with 1:1 ligand ratio of L-/D-cys:MHA. Enantiomer-chiral response relation in Figure 28 induced that the interaction of ligands results in this chiral response.

3.3.1.2 Temperature Dependency of Chirality

Temperature-dependent measurements of chiral response also promoted this idea. We heated the solution of clusters up to 90 °C and observed a decrease in chiral response after 75 °C. At this temperature, the interactions between ligands that lead to chiral response can disintegrate.
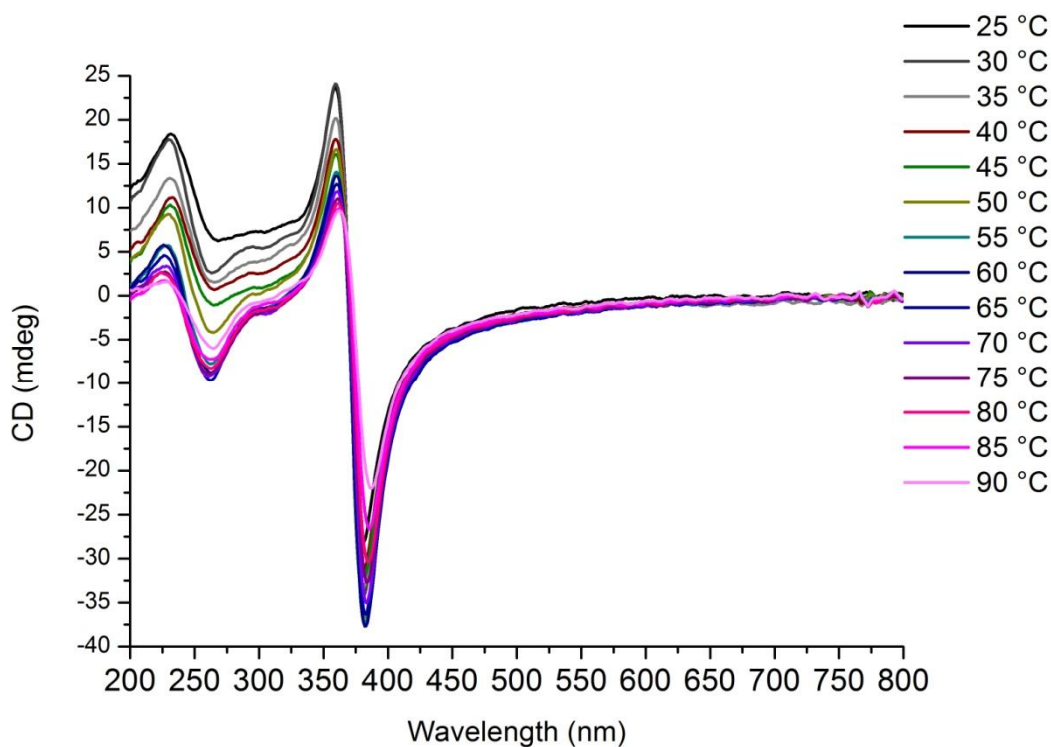
Figure 30: Effect of temperature on the chirality of the nacre samples

3.3.1.3 Effect of Different Silver Precursors on Nacre Formation

We changed silver precursor, to check the role of silver nitrate in iridescent structure formation. We used silver trifluoroacetate instead of silver nitrate and we observed nacre-like structure, as well. (Figure 31 and Figure 32)
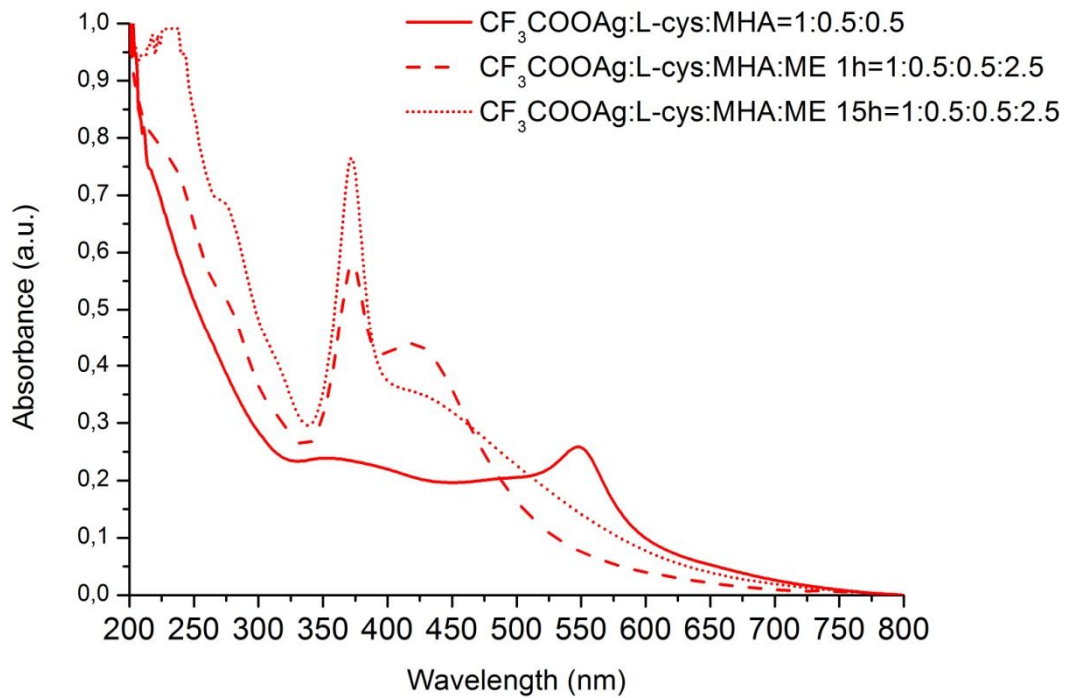
Figure 31: Effect of using silver trifluoroacetate as precursor on the formation of nacre
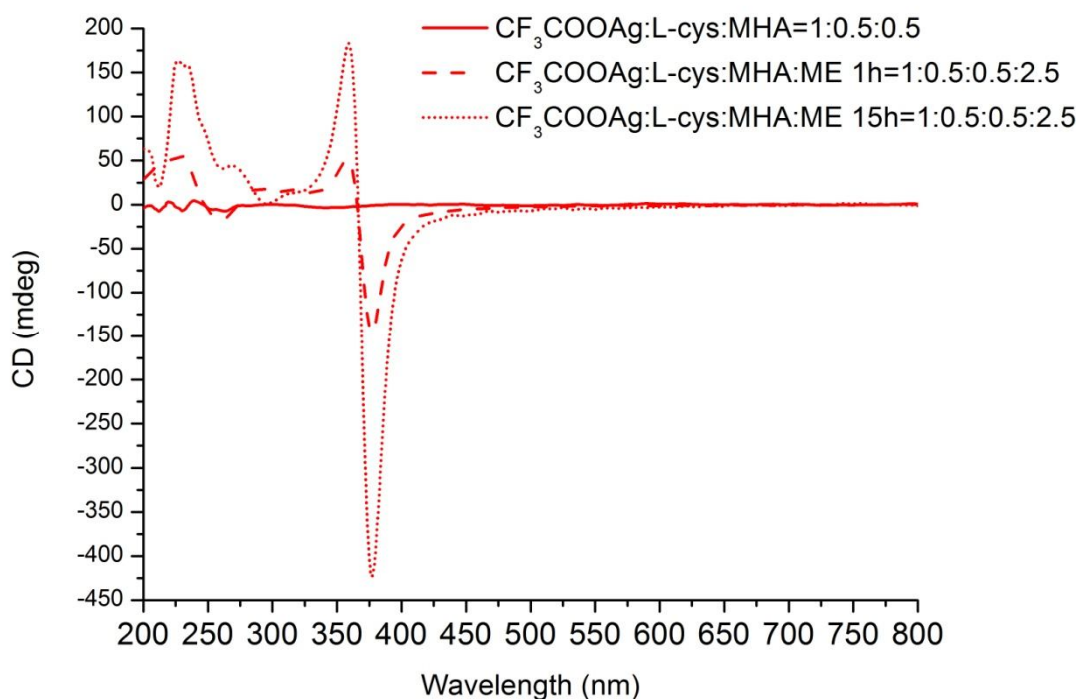
Figure 32: Effect of using silver trifluoroacetate as precursor on the formation of chiral response

3.3.1.4 Effect of Using Different Ligands for Nacre Formation

We also tried different the ligand combinations to see the effect of MHA in this system. We combined mercaptophenylacetic acid (MPAA), mercaptophenol (MP), and mercaptobenzoic acid (MBA) with Cys. Cys to other ligand ratio was kept 1 to 1 to ease comparison. Although they did not form nanoclusters, the prominent peak ~375 nm existed in each combination. Still we observed subtle changes in optical absorption and chiral response peaks. The bulky structures of other ligands can explain these behaviors. (Figure 33 and Figure 34)
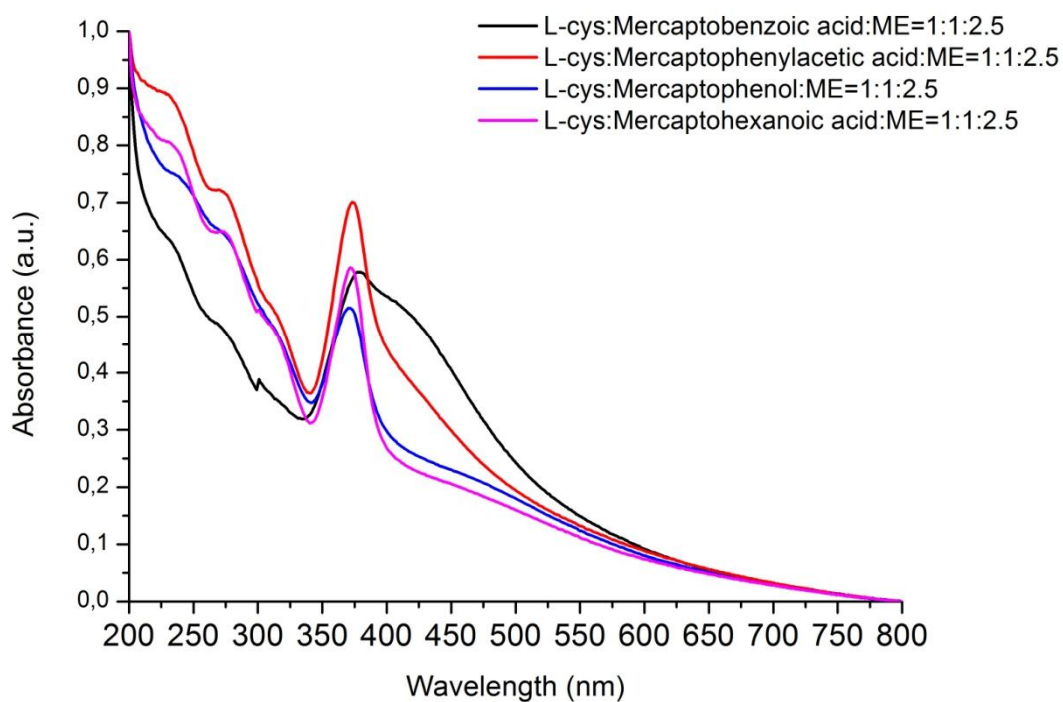
Figure 33: Effect of using different ligands instead of mercaptohexanoic acid on the formation of nacre samples
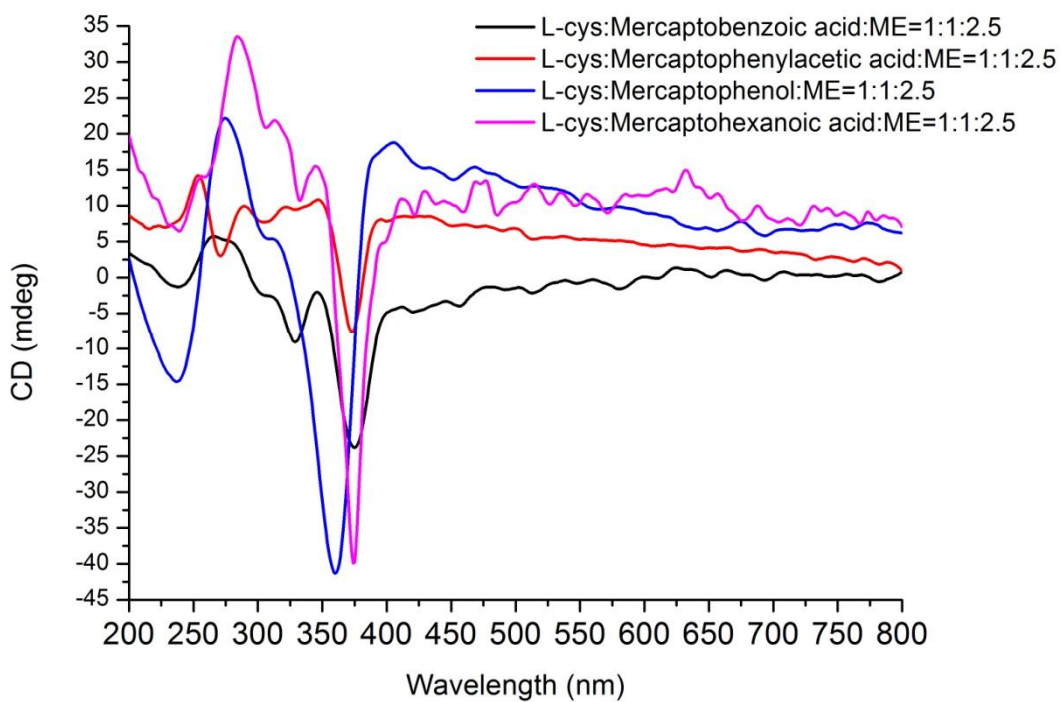
Figure 34: Effect of using different ligands instead of mercaptohexanoic acid on chiral response

We demonstrated that existence of mixed ligand was not a requirement for the formation of nacre. Still, we utilized pure MBA, MPAA, and MP to synthesize nacre structure. Although they did not induce identical absorption spectra, existence of the prominent peaks ~375 nm pointed the formation of nacre. (Figure 35) The sample with pure MBA had a spectrum with a red shift and broadness, but still the iridescent color was observed even in this solution. (Figure 37) Among all of the ligands, Cys lead to most pronounced chiral response. The noisy spectra which we observed can be resulted from the non-equally dispersed bulky particles in the solution. (Figure 36)
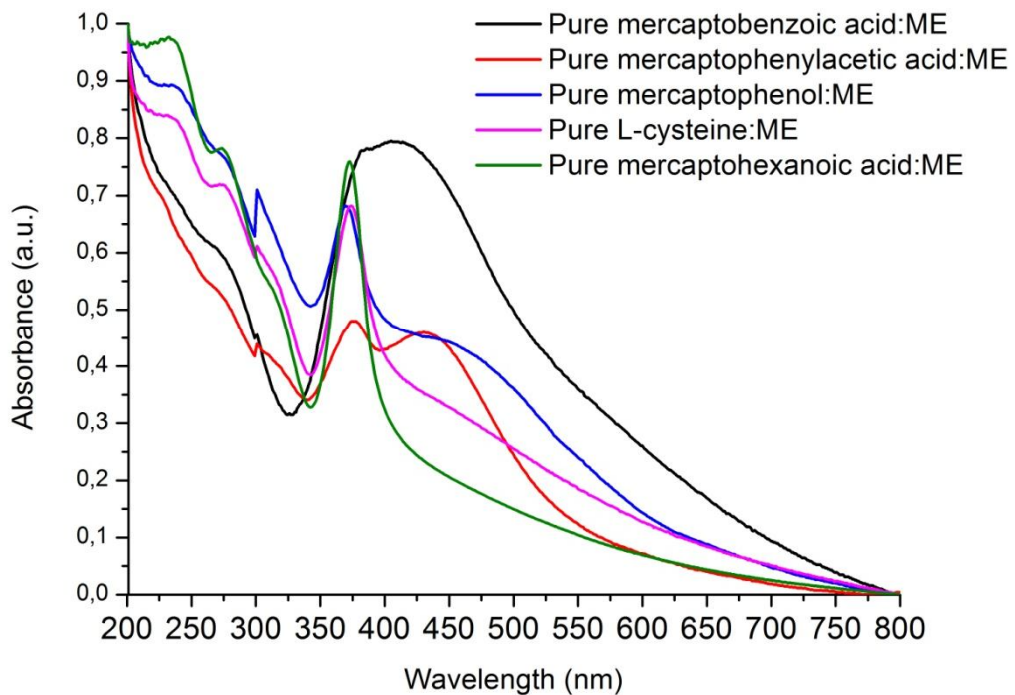
Figure 35: Effect of using pure ligands on formation of nacre structure
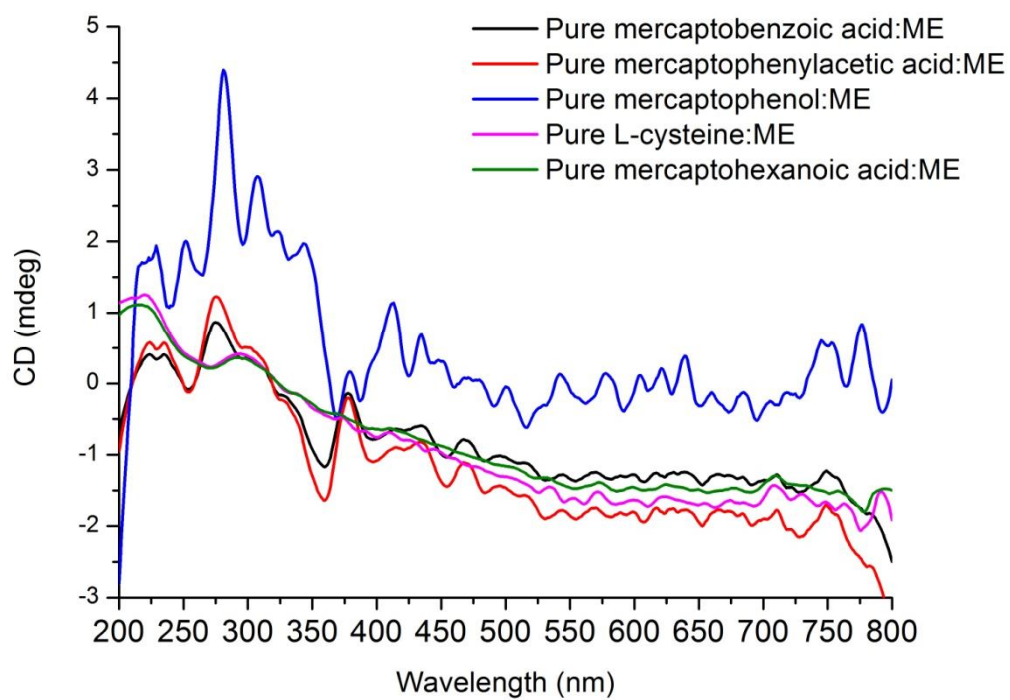
Figure 36: Effect of using pure ligands on chiral responses

Figure 37: Dark color of nacre structure that was synthesized with pure MBA

3.3.1.5 Effect of Mercaptoethanol Amount on Nacre Formation

In order to examine the effect of excess amount of ME, we increased the amount 10 times compared to ratio of silver:ME that is 1 to 2.5 in initial experiment. Although we monitored the prominent peak ~375 nm after an hour, there was no chiral response in CD measurements. (Figure 39) While chiral response measurement was consistent after 18 hours, sample did not provide the prominent peak in absorption spectrum. (Figure 38) We can speculate about ligand interactions that may be disintegrated leading disappearance of previous chiral response and absorption.
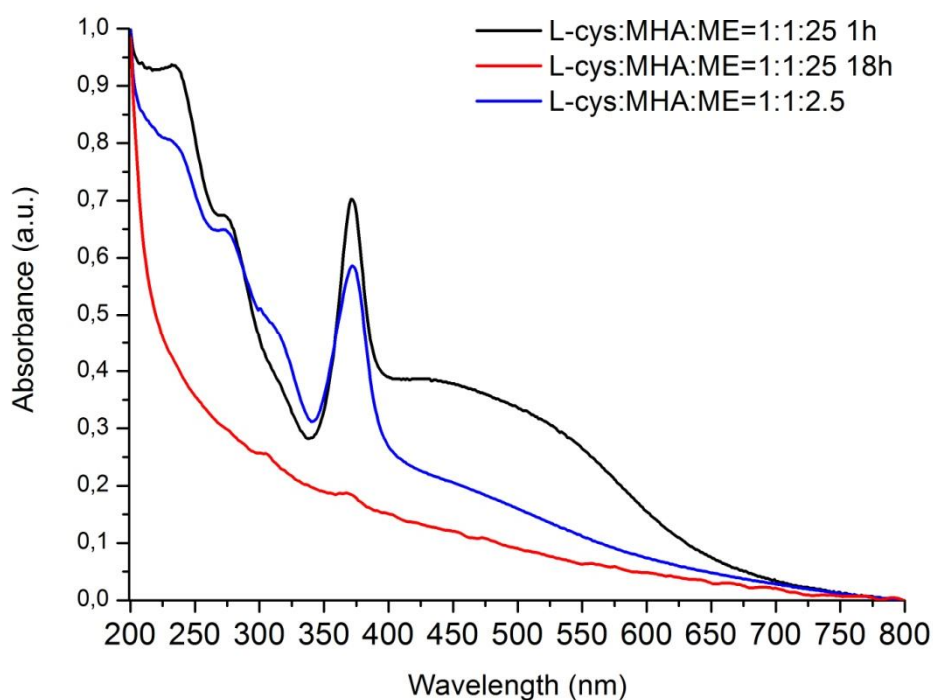
Figure 38: UV-vis spectra of nacre with excess amount of mercaptoethanol
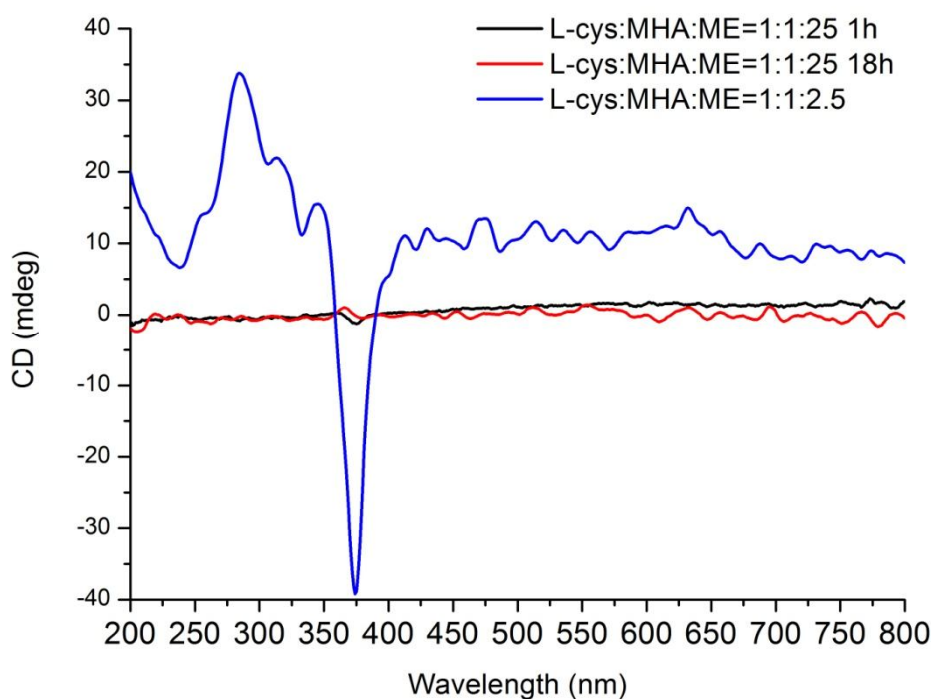
Figure 39: CD spectra of nacre with excess amount of mercaptoethanol

3.3.1.6 Effect of Reducing Agents on Nacre Formation

ME is a weak reducing agent compared to sodium borohydride ($NaBH_4$). As an aggressive reducing agent $NaBH_4$ is often used to produce nanostructures from precursors. In comparison to $NaBH_4$, ME is more likely to form particles slower which can allow to a hierarchical structure to be formed. Hence, instead of $NaBH_4$, we utilized ME as primary reducing agent. After an hour we observed the formation of nacre structure with a brighter, white color and UV-vis spectrum also proved the formation of nacre. (Figure 40) Additionally, we monitored chiral response in CD spectroscopy. (Figure 41) In order to follow the synthesis routine, after 5 hour we added $NaBH_4$ leading an instant color change to dark brown. This phenomenon is related the reduction of silver precursor. While the absorption around prominent peak increased a lot, chiral response varied insignificantly and then decreased drastically after 18 hours. Form of UV-vis spectrum changed significantly after 18 hours leading speculations of agglomeration.
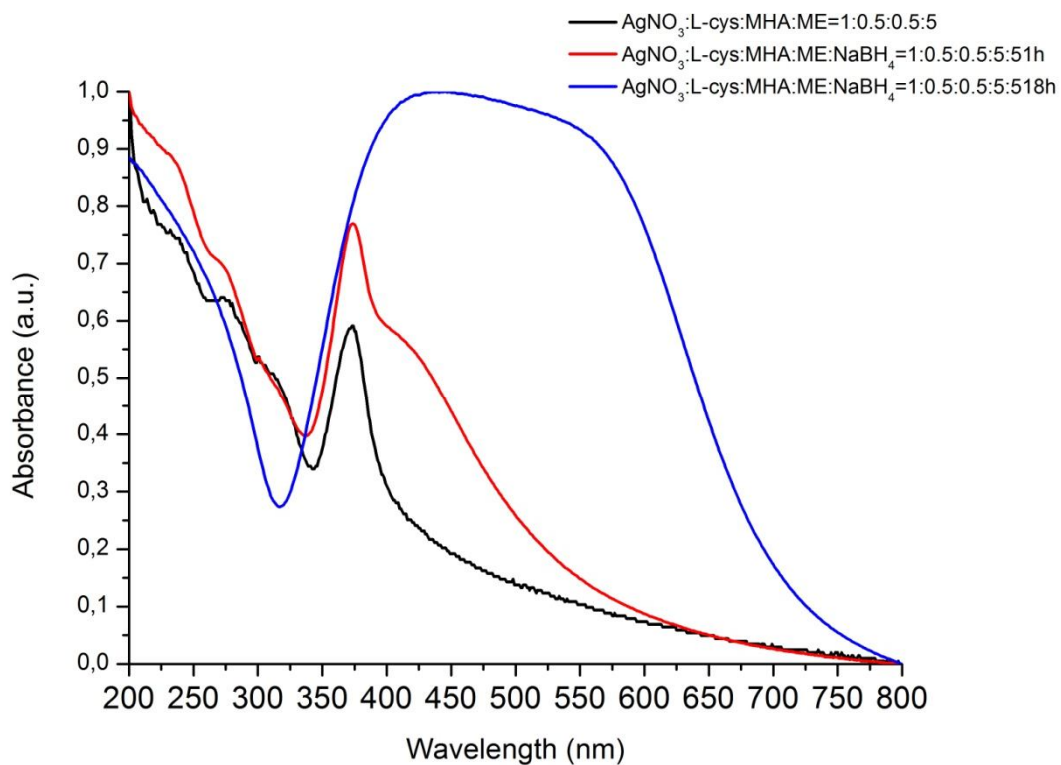
Figure 40: UV-vis spectra of samples which were reduced with mercaptoethanol instead of NaBH$_4$
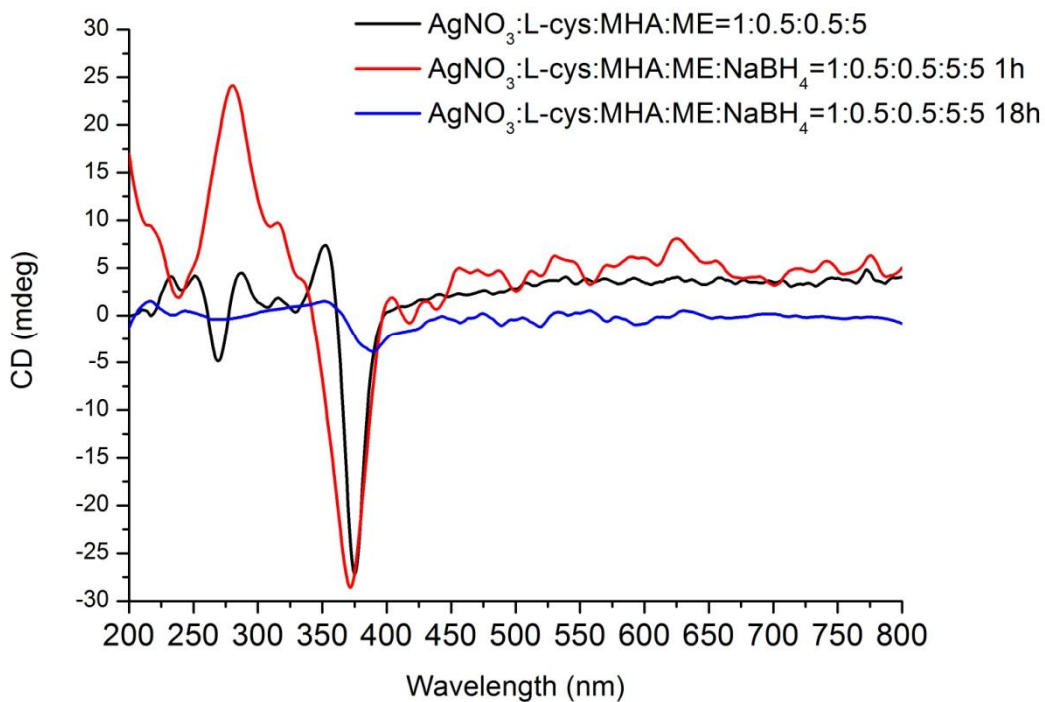
Figure 41: CD spectra of samples which were reduced with mercaptoethanol instead of NaBH

3.3.2 Crystallographic Properties

To study structural properties of nacre-like structures, we used x-ray diffraction (XRD) spectroscopy. (Specifications of measurements are provided in Chapter 4) Samples were prepared by drop casting of samples on glass slides. Nacre-like structures with different ligand ratios were examined and three distinct crystal peaks between 2 and 26 (2θ) degrees were monitored. All samples provided the same diffraction regardless of ligand ratio. (Figure 42) The not-broad shapes of peaks in the spectra indicated the formation of big crystal parts in the system. Also amount of peaks shows two levels of periodicity which can form a hierarchical structure just as brick-mortar structure of nacre. We can speculate that drying process of nacre constructed this alignment of repetitive parts.
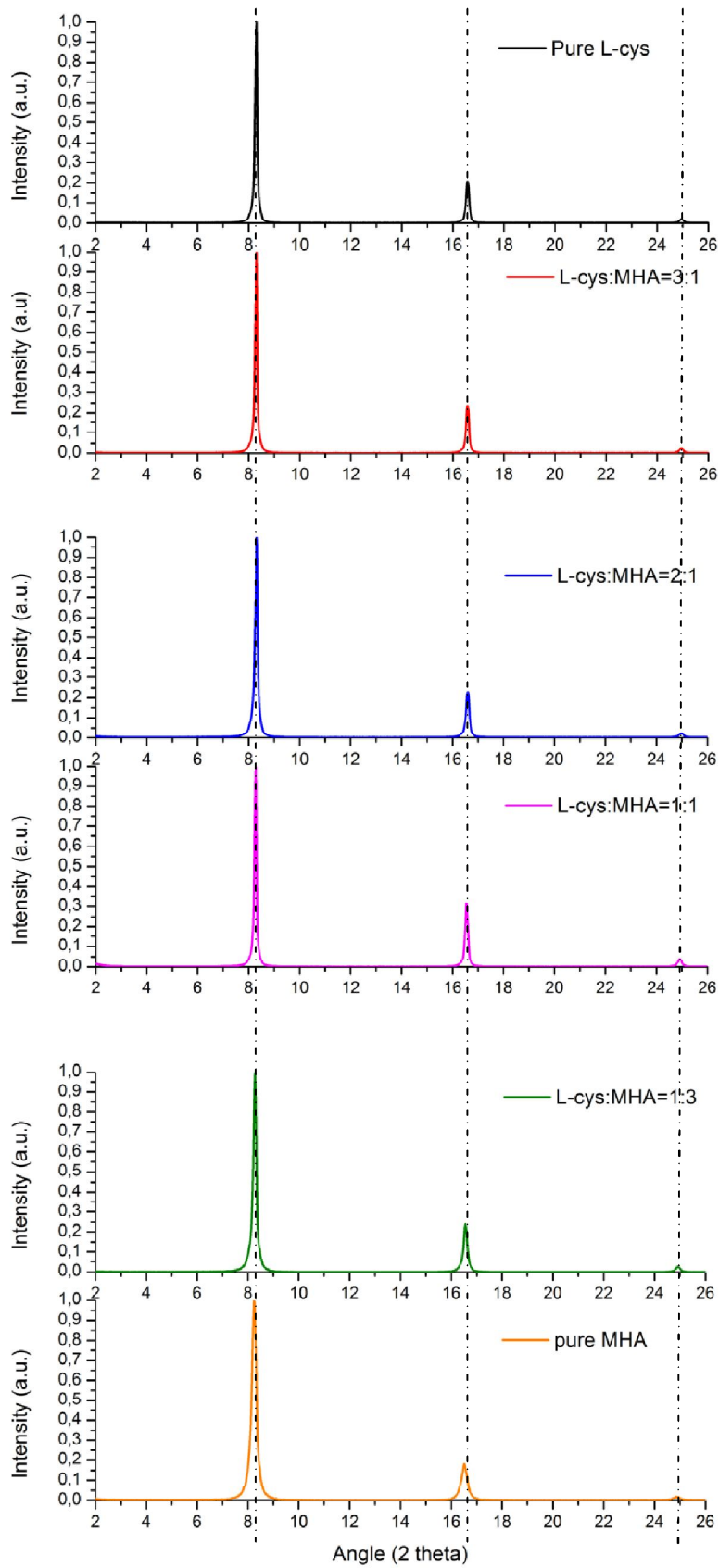
Figure 42: X-ray spectroscopy on nacre structures of different ligand ratios

When we changed the ligands, we also observed three prominent yet shifted peaks that induce the formation of lamellar structure. (Figure 43) Different amount of carbons may affect the formation crystallographic properties as well as the distance between these crystals in nacre-like structures.
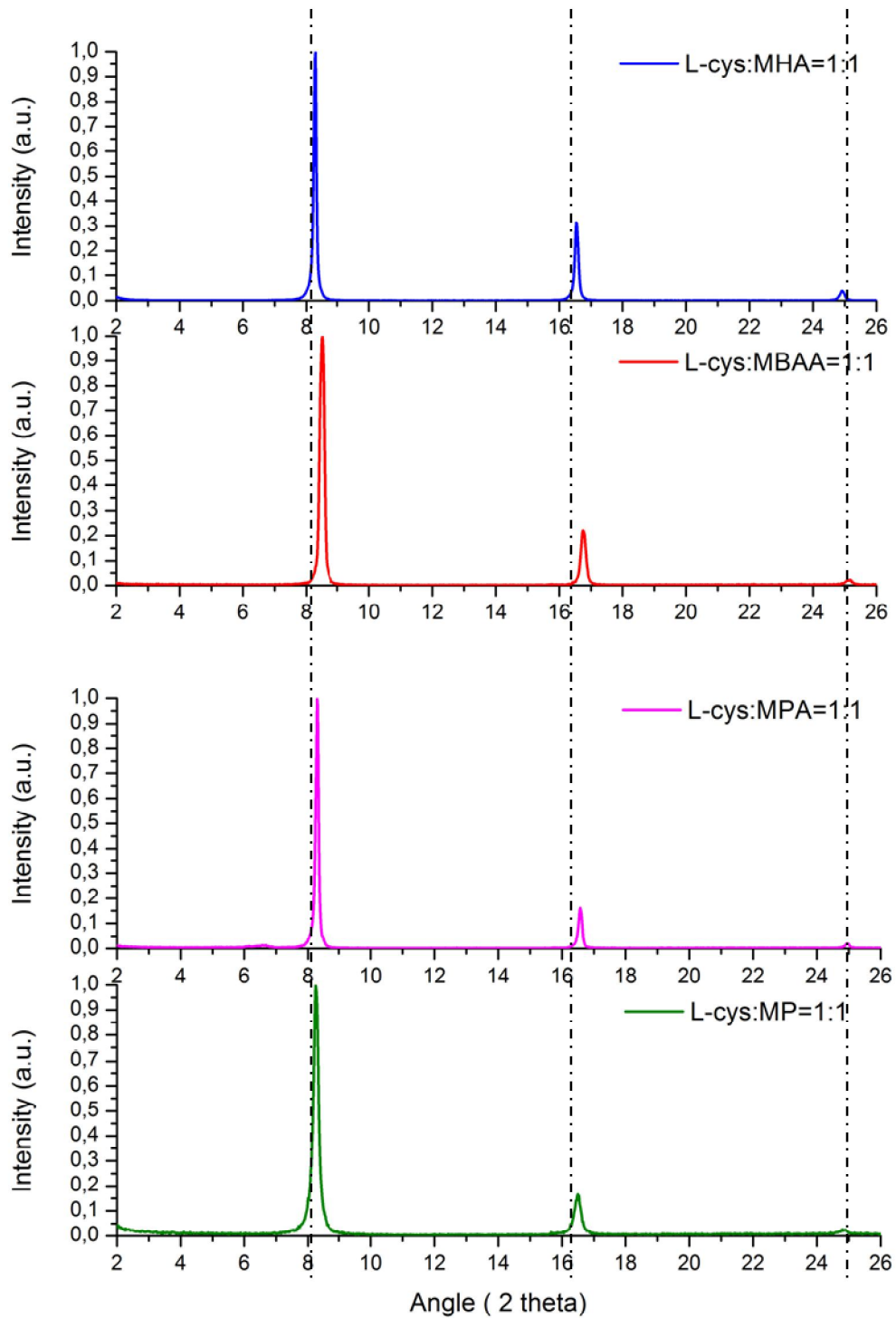
Figure 43: X-ray spectroscopy on nacre samples with different ligand combinations

Figure 44 shows the crystal structure did not change with existence of excess amount of ME. Additionally, when the precursor was reduced with ME instead of $NaBH_4$, there was no change on crystal properties.
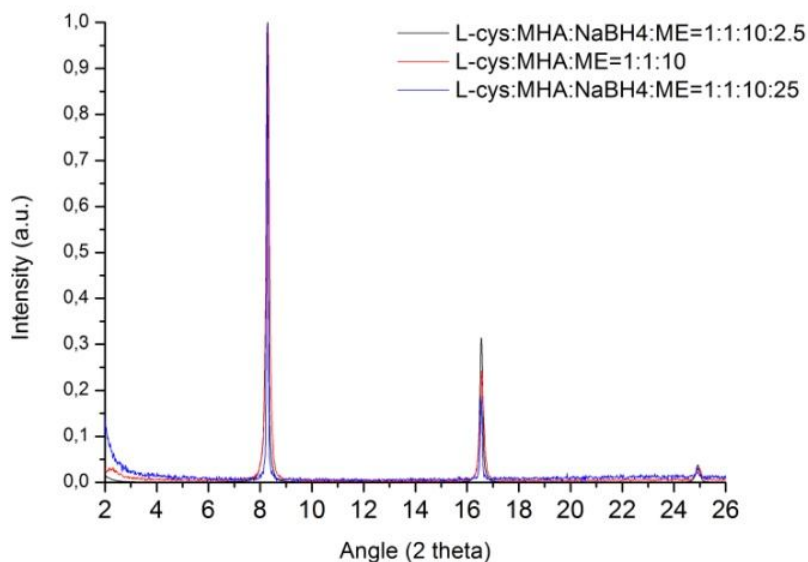
Figure 44: X-ray spectroscopy on nacre samples with excess amount of mercaptoethanol and directly reduced with mercaptoethanol instead of $NaBH_4$

3.3.3 Scanning Electron Microscopy

Microscopy is crucial to elucidate properties about structures. We prepared the samples by drop cast method on silica wafers. To compare the probable ligand effect on structure one nacre sample with mixed ligand and one with pure ligand systems were examined. In both samples we observed a structure with a plenty amount of buds. (Figure 45)
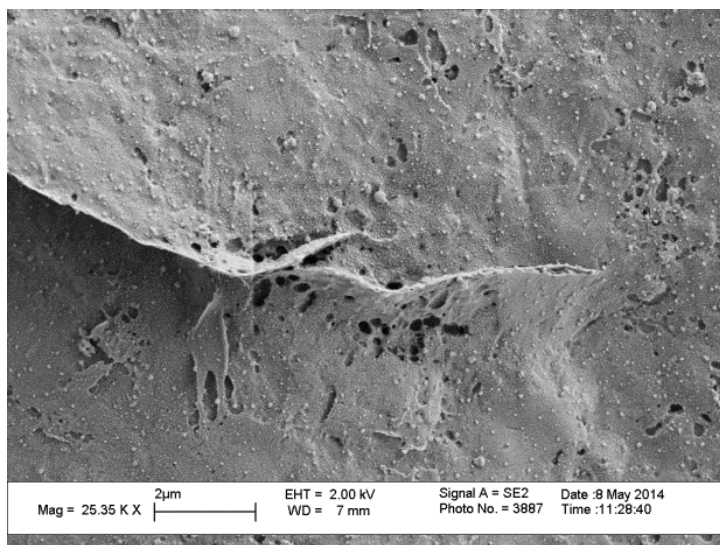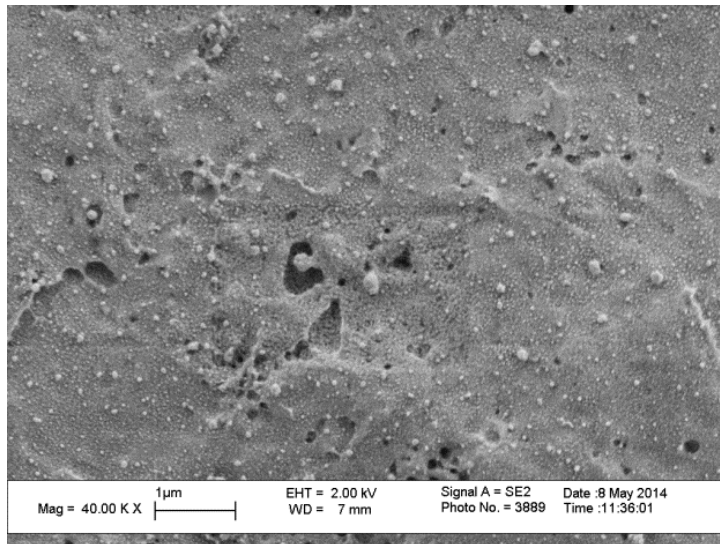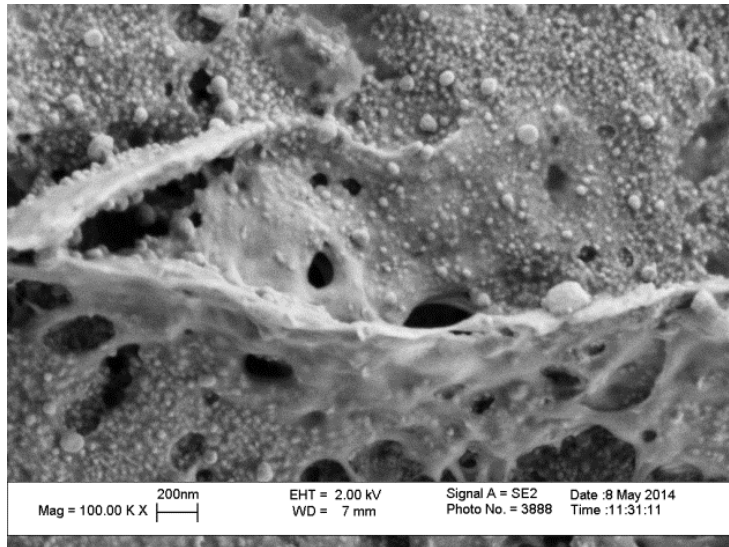
Figure 45: SEM images of nacre sample with pure L-cys

There were some parts that we assumed a result of drying effect such as structure in Figure 46 which looks like wrapped paper. With higher magnifications, resemblance to the texture in Figure 45 in terms of buds appeared. (Figure 46)
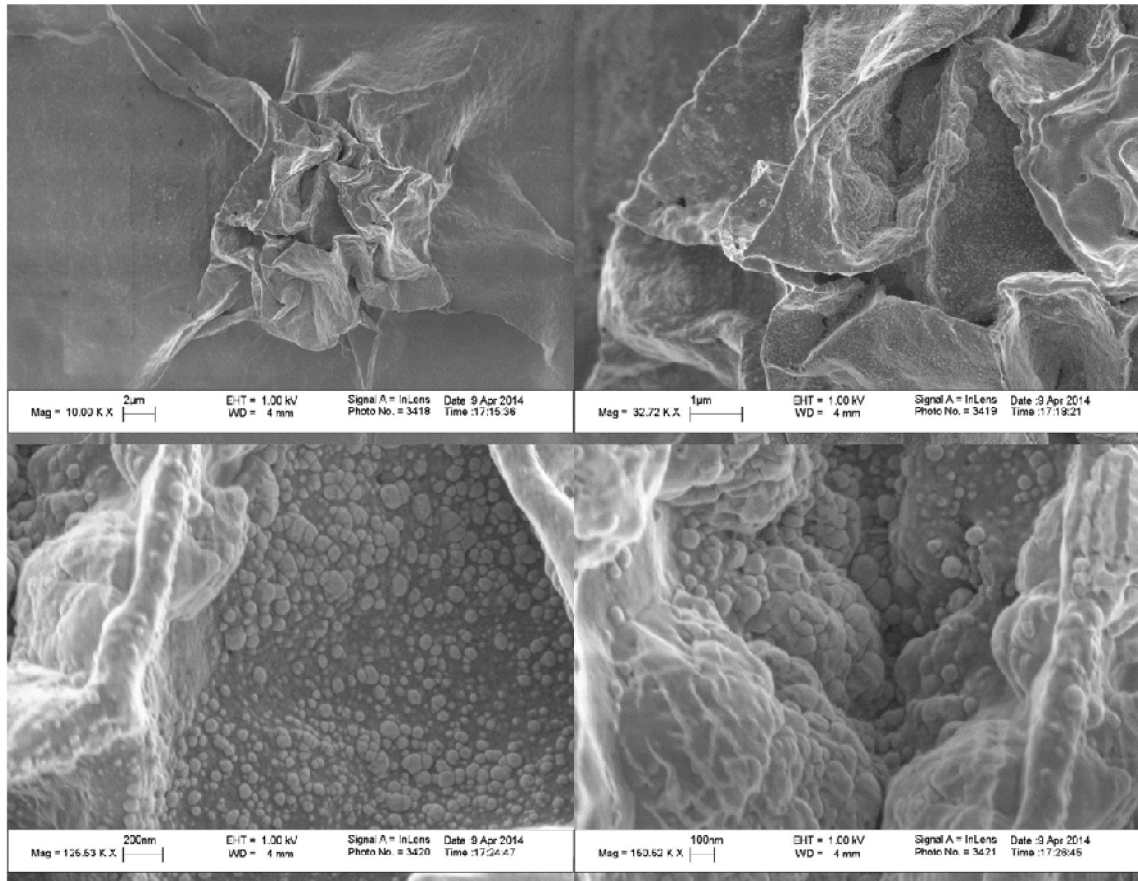
Figure 46: SEM images of nacre sample with a 1 to 1 ratio of L-cys:MHA

3.3.4 Electrical Properties

Since the main part of the nacre-like structure is based on metal, in order to check whether the nacre structure is conductive, small parts of glass were coated with 3 different nacre solutions via drop casting. All three samples had 1 to 1 L-cys:MHA ratio with different ME amounts and one of the samples was reduced by ME. Conductivity of the samples was measured as a current/voltage reaction to a current/voltage stimulus. A basic set-up with voltage/current source, voltage/current meter, switches, and clamps

was used. We monitored their reactions to stimuli and only nacre sample with excess amount of ME induced a response. (Figure 49)
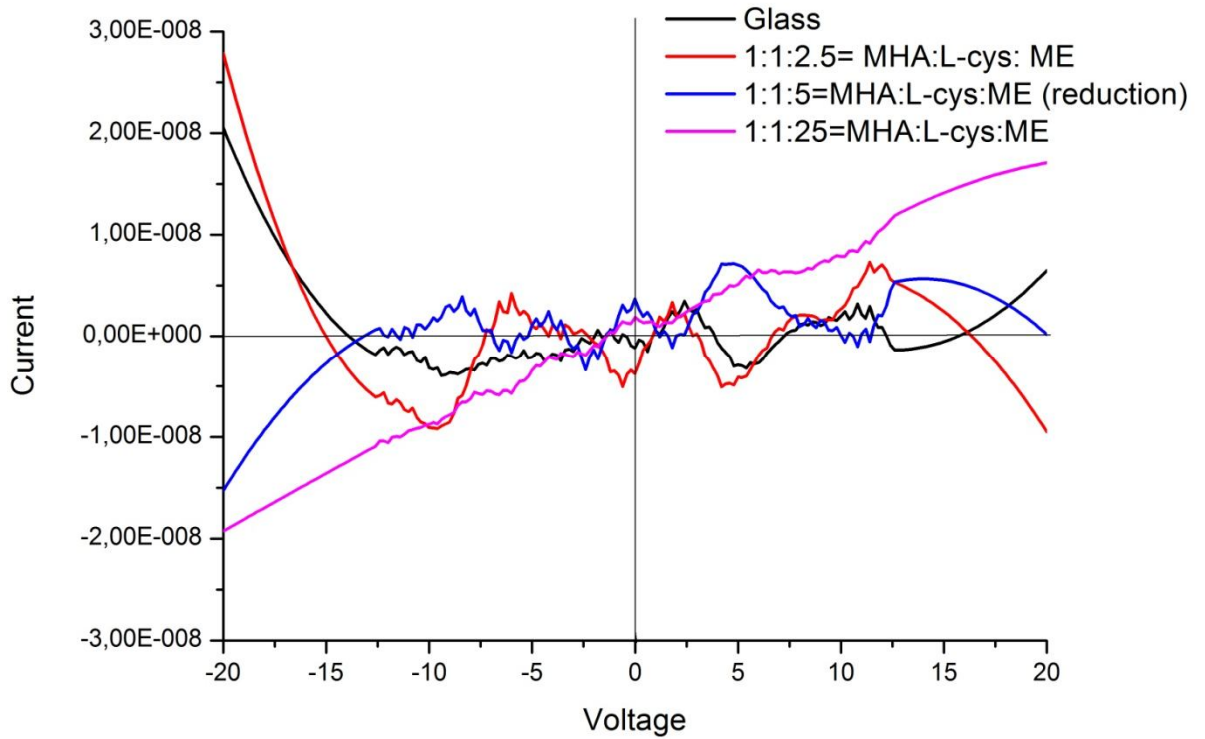
Figure 47: Voltage vs Current graph for glass parts coated with 3 different nacre solutions

CHAPTER 4

EXPERIMENTAL

4.1 Chemicals

Silvernitrate was purchased from Alfa Aesar. L , D-cystein (Cys), 6-Mercaptohexanoic acid (MHA), sodium borohydrate, methanol, sodium hydroxide, 4-mercaptophenol (MP), 4-mercaptophenylacetic acid (MPAA), mercaptobenzoic acid (MBA), and 2-mercaptoethanol (ME) were purchased from Sigma Aldrich. The all chemicals were used without any further purification. The chemical structures for ligands are given in Figure 50.

D, L-Cysteine   6-Mercaptohexanoic acid

4-Mercaptobenzoic acid   4-Mercaptophenol

2-Mercaptoethanol   4-Mercaptophenylacetic acid
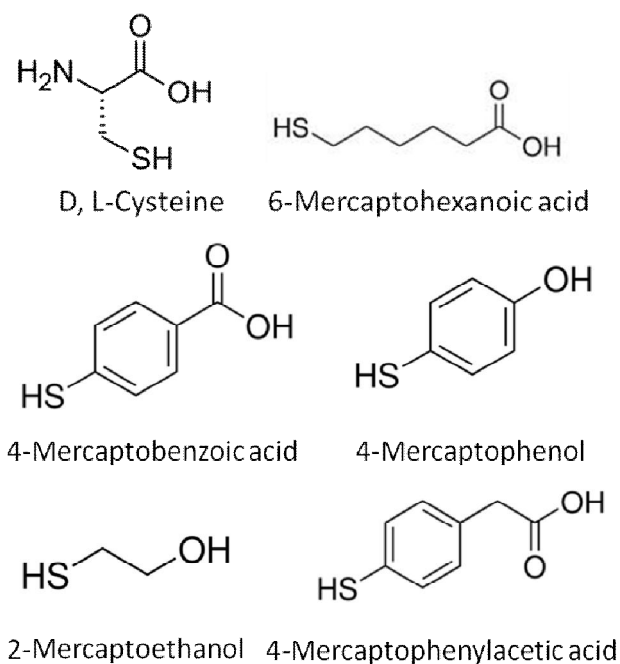
Figure 48: Molecular structure of ligands used in formation of nanoclusters and nacre samples

4.2 Synthesis

We synthesized mixed ligand silver nanoclusters by reducing silver nitrate in methanol and water mixture at room temperature (RT). We used double distilled water throughout the experiments. First, we mixed equal volumes (12.5 ml) of methanol and water; purged this mixture with nitrogen and adjusted its pH to 11 by adding sodium hydroxide solution. We dissolved 4.45 mg (0.036 mmol) of L-cys in this solution and then added 5.08μl (0.036 mmol) of MHA.

In silver to thiol ligand ratio of 1, we used 12.5 mg (0.073 mmol) of silver nitrate and reduced silver by addition of 13.91 mg (0.36 mmol) sodium borohydride in water. We kept the reaction under vigorous stirring for 6 hours. The color of the solution became yellow immediately and gradually turned into dark brown, then into red/pink. To end the reaction, we precipitated the product by the addition of tetrahydrofuran (THF) and concentrated the precipitate in water through centrifugation.

We followed the same procedure to synthesize nanoclusters with different ligand ratios of L-cys:MHA (1:2, 1:3, 2:1, and 3:1) at a single silver to thiol ratio (1:1). We also changed the silver to thiol ratio to track the formation of nanoclusters.

To synthesize nacre-like structures we used 10.32 μl of ME to the above mentioned reaction after 5 hours. To use ME as the principle reducing agent, we used a ratio of 1:5 for silver to ME ratio.

4.3 Post-processing After Synthesis

We separated the raw product using PAGE (Cleaver, OmniPAGE mini vertical electrophoresis system) with a separating gel of 30% and a stacking gel of 8% acrylamide monomers (acrylamide/bisacrylamide=93/7), respectively. The size of the gel was 10 cm × 10 cm × 2 mm. We used a buffer solution of Tris-HCl with pH 8.8 for the separating gel and pH 6.8 for the stacking gel. The running electrode buffer was an aqueous mixture of glycine (192 mM) and Tris (25 mM). We took 1 ml of the reaction mixture, precipitated the product in THF,

redissolved it in 50 µl water, and added 16 % (v/v) of glycerol to this solution. We loaded 5 µl of this solution into the well of the stacking gel and eluted the sample for 3 hours at 4°C with constant 200 V (Cleaver, CS-300V) to separate the product. To extract silver nanoclusters, we cut the bands at each fraction and left them in water for a day. We used filters with 0.2 µm pore size to remove remaining lumps of gel. The extracted nanoclusters are kept in room temperatures in sealed eppendorf tubes.

4.4 Characterization

4.4.1   Circular Dichroism Spectroscopy

We measured absorption of chiral formations using Jasco J-810 CD spectrometer. We used quartz cuvettes with 1 mm path length to obtain more reliable results.

4.4.2   UV-visible Spectroscopy

We investigated the absorption of the band gaps of silver nanoclusters using UV-Visible (optical) absorption spectroscopy (Shimadzu, UV-3150, Kyoto, Japan). We used quartz cuvettes with 1 mm path length were used in order to avoid absorptions by cuvettes.

4.4.3   Scanning Electron Microscopy

We examined structures of nacre samples using Leo Supra VP35 Field Emission Scanning Electron Microscope and Elemental Analysis Spectrometer. We used secondary electron detector and in lens detector with 1 and 2 eV. We prepared samples by drop casting on silicon wafers and we left them drying at RT.

4.4.4   X-ray Diffraction Spectroscopy

We studied crystalline parts of the nacre structure were studied using Bruker AXS D8 X-ray Diffractometer.We prepared samples by drop casting on glass microscopy slides

and we left them drying at RT. We scanned in each measurement between 2 and 90 degrees (2θ).

4.4.5 Transmission Electron Microscopy

To determine the particle size we used JEOL 2000FX Transmission Electron Microscopy. We prepared our samples via solution dipping of Ted Pella copper grids.

.

CHAPTER 5

FUTURE WORK

The nacre liquid that we synthesized requires further characterizations to understand its structure in detail. Its unique optical and chiroptical properties make it promising for applications such as chiral coatings and chiral sensing. To widen these applications this structure can be utilized in two prominent ways; embedding different materials in nacre structure and optimizing the assembly of nanoparticles in which hierarchical structures can appear.
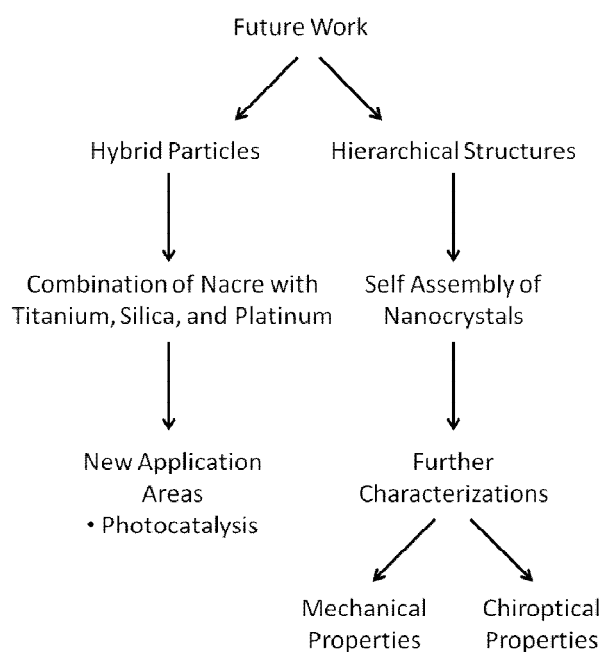
Figure 49: Schematic of future work plan about thesis project

5.1 Hybrid Particles

Hybrid structures combine the characteristics of building blocks leading unique properties. They can be formed with combination of several materials just as bimetallic nanoparticles, metal-semiconductor core-shell structures, and organic-metal nanostructures. Using noble-metals is advantageous in this case due to their Fermi levels which prolong electron-hole lifetime by accumulation of photo-generated electrons [66, 67]. However, noble-metals like gold and platinum are not cost-effective and that is why silver is more preferred. Additionally, optical response of silver is tunable regarding its shape, dimension, and interparticle interaction leading to a widespread utilization in hybrid materials.

Hybrid materials are promising structures for catalytic applications, chemical and biosensing via optical response. Combination of silver and titanium leads an enhanced photocatalytic activity due to high oxidation level of silver. When visible light forms electron-hole pairs in TiO_2, existence of silver prolongs the separated state leading initiation of reactions [66]. High oxidation level and cost-effectiveness make silver as one of the most utilized materials in hybrid structures. Es-Souni forms TiO_2-Ag nanocomposite thin films by using silver's oxidation ability leading formation of self organized silver nanoparticles on TiO_2 [68]. Also another hybrid structure combining silver with silica is used by to enhance thermal conductivity [69].

Hybrid materials such as organic-metal, metal-metal nanostructures can have distinctive absorption peaks in visible region leading to possible sensing applications [70]. We synthesize our structures in high pH and Sugimoto *et al.* showed that pH modifies the shape of TiO_2 particles in synthesis reaction [71]. (Figure 52) Therefore we can combine our nacre structure with different shapes of TiO_2 to form hybrid structures. Additionally, we are planning to modify nacre by combination with silica.
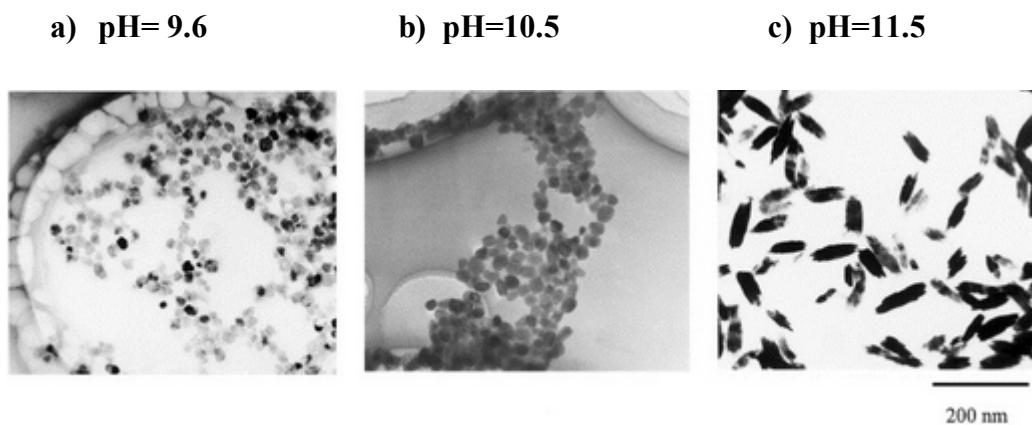
Figure 50: Effect of initial pH on the shape control [71]

5.2 Hierarchical Structure

Nanocrystal assemblies are pronounced due to their modified electronic, optical, and mechanical properties regarding their structure and alignment. Individual crystals can gain unique properties in a 2D or 3D assemblies due to interactions between them. Synthesis of monodisperse particles eases the structure tailoring leading to demanding characteristic properties. In the formation of large crystalline domains, apart from monodispersity of the particles interparticle interactions also contribute to modification of properties. For example, electromagnetic coupling between metallic nanocrystals makes nanocrystal assemblies ideal for plasmonic applications, since it offers narrow plasmon bands and intense field enhancements in the interstitial spaces between adjacent nanocrystals [72]. The latter strengthens optical properties just as resonant light scattering, superlensing, and surface-enhanced Raman scattering.

We have extensive amount of data for chiroptical properties of structures in solution, but as nacre coating. Our preliminary study of solutions on polarized optical microscopy can be extended to coatings of nacre structure. Additionally, nacre coatings on quartz substrates can be subject to solid circular dichroism spectroscopy [73].

We know that chirality of the nacre solution depends on existence of cysteine in the form of different enantiomers. Since there are studies about disappearance of chirality due to cysteine mercury interaction [74] and enantioselective interaction between cysteine and carnitine [75], we can investigate the utilization of these interaction with our coatings.

53

Controlling interparticle spacing, density, and packing symmetry in these structures also increases the tunability in properties. In intertwinned colloid lattices control over construction of permeation of the structures can create macroscopic optomechanical structures in which physical stimuli like shear torsion results in color change leading promising applications as smart textiles and responsive environmental sensor [76].

Although optical properties are studied in advance, mechanical properties are rarely investigated. Sader, *et al.* supposed to use microfabricated levers or beams as measuring devices to measure Elastic modulus of a photonic crystal [77]. Microcantilever of AFM has a vibration frequency in terms of its width, length, Young's modulus, and beam density. When a photonic crystal grows on the cantilever, the change in the frequency correlates with Young's modulus of the crystal which provides data about interparticle adhesive forces [76].

To acquire hierarchical structures there are several processes. For example Salgueirino, *et al.* used layer by layer assembly to form a hierarchical structure with silver and silica [78]. Additionally, Langmuir-Blodgett assembly, electrophoretic deposition, solution dipping, and template inhibition are common for assembling [51]. To characterize hierarchical structures SAXS can be utilized.

5.2.1 Small Angle X-ray Scattering (SAXS)

SAXS is a fundamental characterization tool to analyze structure of condensed matter. Measurements are carried out by scanning a range of low angles (e.g., 0.1-10°). Materials such as metal alloys, synthetic polymers in solution or in bulk, biological macromolecules in solution, and nanoparticles have been subject to investigation with SAXS [79]. SAXS was invented by Guinier following his studies with metallic alloys [80]. It bases on scattering of small angle x-rays that are close to primary beam from the sample leading the structural information. (Figure 53) The scattering signal is developed from the difference in the average electron density, $\Delta\rho(r)$, of solute molecules of interest, $\rho(r)$, and bulk solvent ρ_s: [81]

$$\Delta\rho(r) = \rho(r) - \rho_s$$
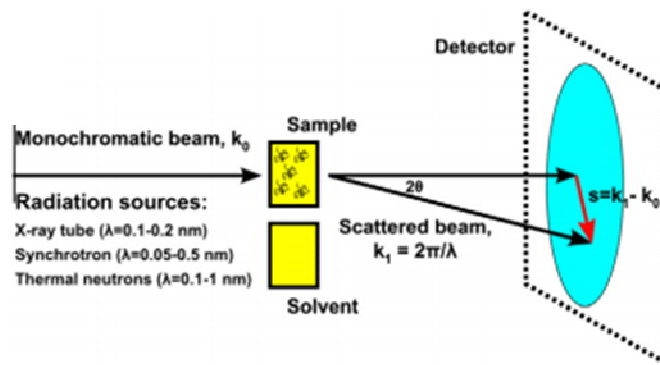
Figure 51: Schematic illustration of SAXS experiment [82]

Apart from size and shape of the particles, SAXS provides information about internal structure of disordered and partially ordered systems. Scattering of patterns in the solution is symmetric due to their tumbling in the solution. Since it is possible to have information about intermolecular interactions such as assembly and large-scale conformational changes [79], SAXS is crucial for our further characterization plans about nacre. Due to our preliminary SAXS data, we speculate that our nacre sample have hierarchical structure.

In nature nacre is one of most prominent example of hierarchical structure. Although there are studies synthesizing nacre-like structures with non-metallic materials, metal based nacre is pioneered in our research. To widen its application, regarding the previous characterization techniques on likely structures, we are planning to measure mechanical properties and combine it with other prominent materials to form hybrid structures with unique properties. Additionally, we plan to use platinum to construct nacre-like structure. Although formation of nanoclusters is not required for the formation of nacre structure, we believe that hierarchical assemblies of nanoclusters can lead unique properties such as catalysis due to high surface area.

REFERENCES

1.   Pool, R., *Clusters: Strange Morsels of Matter: When metals or semiconductors are shrunk down to clumps only 10 or 100 atoms in size, they become a" totally new class of materials" with potentially valuable applications.* Science (New York, NY), **1990**. 248(4960): p. 1186.

2.   Jones, M.R., et al., *Templated techniques for the synthesis and assembly of plasmonic nanostructures.* Chemical reviews, **2011**. 111(6): p. 3736-3827.

3.   Willets, K.A. and R.P. Van Duyne, *Localized surface plasmon resonance spectroscopy and sensing.* Annu. Rev. Phys. Chem., **2007**. 58: p. 267-297.

4.   Aikens, C.M., *Electronic Structure of Ligand-Passivated Gold and Silver Nanoclusters.* The Journal of Physical Chemistry Letters, **2010**. 2(2): p. 99-104.

5.   Wilcoxon, J.P. and B.L. Abrams, *Synthesis, structure and properties of metal nanoclusters.* Chemical Society Reviews, **2006**. 35(11): p. 1162-1194.

6.   Fedlheim, D.L. and C.A. Foss, *Metal nanoparticles: synthesis, characterization, and applications*. **2001**: CRC Press.

7.   Shi, Q. and G. Jackowski, *One-dimensional polyacrylamide gel electrophoresis.* Gel electrophoresis of proteins: A practical approach, 3rd ed. Oxford University Press, Oxford, **1998**: p. 1-52.

8.   *A Guide to Polyacrylamide Gel Electrophoresis and Detection*. [cited 2014 July, 1]; Available from: http://www.bio-rad.com/webroot/web/pdf/lsr/literature/Bulletin_6040A.pdf.

9.   Brack, M., *The physics of simple metal clusters: self-consistent jellium model and semiclassical approaches.* Reviews of Modern Physics, **1993**. 65(3): p. 677.

10.   Watzky, M.A. and R.G. Finke, *Transition metal nanocluster formation kinetic and mechanistic studies. A new mechanism when hydrogen is the reductant: slow,*

continuous nucleation and fast autocatalytic surface growth. Journal of the American Chemical Society, **1997**. 119(43): p. 10382-10400.

11.   Bakr, O.M., et al., *Silver Nanoparticles with Broad Multiband Linear Optical Absorption.* Angewandte Chemie, **2009**. 121(32): p. 6035-6040.

12.   Harkness, K.M., et al., *Ag44(SR)304-: a silver-thiolate superatom complex.* Nanoscale, **2012**. 4(14): p. 4269-4274.

13.   Yang, H., et al., *All-thiol-stabilized Ag44 and Au12Ag32 nanoparticles with single-crystal structures.* Nature communications, **2013**. 4.

14.   Schmid, G., *Clusters and colloids: bridges between molecular and condensed material.* Endeavour, **1990**. 14(4): p. 172-178.

15.   Jiang, S., et al., *Janus Particle Synthesis and Assembly.* Advanced Materials, **2010**. 22(10): p. 1060-1071.

16.   Lattuada, M. and T.A. Hatton, *Synthesis, properties and applications of Janus nanoparticles.* Nano Today, **2011**. 6(3): p. 286-308.

17.   Song, F., A. Soh, and Y. Bai, *Structural and mechanical properties of the organic matrix layers of nacre.* Biomaterials, **2003**. 24(20): p. 3623-3631.

18.   Carney, R.P., et al., *Electrical Method to Quantify Nanoparticle Interaction with Lipid Bilayers.* ACS Nano, **2012**. 7(2): p. 932-942.

19.   Cathcart, N. and V. Kitaev, *Silver Nanoclusters: Single-Stage Scaleable Synthesis of Monodisperse Species and Their Chirooptical Properties†.* The Journal of Physical Chemistry C, **2010**. 114(38): p. 16010-16017.

20.   Liu, X., Y. Hu, and F. Stellacci, *Mixed-Ligand Nanoparticles as Supramolecular Receptors.* Small, **2011**. 7(14): p. 1961-1966.

21.   Pasteur, L., *Recherches sur les relations qui peuvent exister entre la forme cristalline: la composition chimique et les sens de la polarisation rotatoire.* **1848**: Bachelier.

22.   Che, S., et al., *Synthesis and characterization of chiral mesoporous silica.* Nature, **2004**. 429(6989): p. 281-284.

23.   Sánchez-Castillo, A., C. Noguez, and I.L. Garzón, *On the Origin of the Optical Activity Displayed by Chiral-Ligand-Protected Metallic Nanoclusters.* Journal of the American Chemical Society, **2010**. 132(5): p. 1504-1505.

24.   Shemer, G., et al., *Chirality of Silver Nanoparticles Synthesized on DNA.* Journal of the American Chemical Society, **2006**. 128(34): p. 11006-11007.

25.   Guerrero-Martínez, A., et al., *From individual to collective chirality in metal nanoparticles.* Nano Today, **2011**. 6(4): p. 381-400.

26.   Noguez, C. and I.L. Garzon, *Optically active metal nanoparticles.* Chemical Society Reviews, **2009**. 38(3): p. 757-771.

27.   Yao, H., et al., *Large optical activity of gold nanocluster enantiomers induced by a pair of optically active penicillamines.* Journal of the American Chemical Society, **2005**. 127(44): p. 15536-15543.

28.   Nishida, N., et al., *Synthesis and Chiroptical Study of d/l-Penicillamine-Capped Silver Nanoclusters.* Chemistry of Materials, **2007**. 19(11): p. 2831-2841.

29.   Goldsmith, M.-R., et al., *The chiroptical signature of achiral metal clusters induced by dissymmetric adsorbates.* Physical Chemistry Chemical Physics, **2006**. 8(1): p. 63-67.

30.   Gautier, C. and T. Bürgi, *Chiral Inversion of Gold Nanoparticles.* Journal of the American Chemical Society, **2008**. 130(22): p. 7077-7084.

31.   Yao, H., T. Fukui, and K. Kimura, *Chiroptical responses of D-/L-penicillamine-capped gold clusters under perturbations of temperature change and phase transfer.* The Journal of Physical Chemistry C, **2007**. 111(41): p. 14968-14976.

32.   Tamura, M. and H. Fujihara, *Chiral Bisphosphine BINAP-Stabilized Gold and Palladium Nanoparticles with Small Size and Their Palladium Nanoparticle-Catalyzed Asymmetric Reaction.* Journal of the American Chemical Society, **2003**. 125(51): p. 15742-15743.

33.   Cathcart, N., et al., *Chiral Thiol-Stabilized Silver Nanoclusters with Well-Resolved Optical Transitions Synthesized by a Facile Etching Procedure in Aqueous Solutions.* Langmuir, **2009**. 25(10): p. 5840-5846.

34.   Farrag, M., M. Tschurl, and U. Heiz, *Chiral Gold and Silver Nanoclusters: Preparation, Size Selection, and Chiroptical Properties.* Chemistry of Materials, **2013**. 25(6): p. 862-870.

35.   Yao, H., M. Saeki, and K. Kimura, *Induced Optical Activity in Boronic-Acid-Protected Silver Nanoclusters by Complexation with Chiral Fructose†.* The Journal of Physical Chemistry C, **2010**. 114(38): p. 15909-15915.

36.   *Circular Dichroism (CD) and Optical Rotatory Dispersion (ORD).* [cited 2014 June, 26]; Available from: http://www.chem.iitkgp.ernet.in/faculty/SDG/Spectroscopy%20CD.pdf.

37.   *THE CD1 BEAM LINE ON ASTRID.* [cited 2014 July,2]; Available from: http://www.isa.au.dk/facilities/astrid/beamlines/cd1/cd1_3.asp.

38.   Adler, A.J., N.J. Greenfield, and G.D. Fasman, *[27] Circular dichroism and optical rotatory dispersion of proteins and polypeptides.* Methods in enzymology, **1973**. 27: p. 675-735.

39.   Schaaff, T.G. and R.L. Whetten, *Giant Gold−Glutathione Cluster Compounds: Intense Optical Activity in Metal-Based Transitions.* The Journal of Physical Chemistry B, **2000**. 104(12): p. 2630-2641.

40. Yao, H., N. Nishida, and K. Kimura, *Conformational study of chiral penicillamine ligand on optically active silver nanoclusters with IR and VCD spectroscopy.* Chemical Physics, **2010**. 368(1–2): p. 28-37.

41. Román-Velázquez, C.E., C. Noguez, and I.L. Garzón, *Circular Dichroism Simulated Spectra of Chiral Gold Nanoclusters: A Dipole Approximation.* The Journal of Physical Chemistry B, **2003**. 107(44): p. 12035-12038.

42. Kelvin, W.T.B., *Baltimore lectures on molecular dynamics and the wave theory of light.* **1904**: CJ Clay and Sons.

43. Nishida, N., H. Yao, and K. Kimura, *Chiral Functionalization of Optically Inactive Monolayer-Protected Silver Nanoclusters by Chiral Ligand-Exchange Reactions.* Langmuir, **2008**. 24(6): p. 2759-2766.

44. Creighton, J.A., C.G. Blatchford, and M.G. Albrecht, *Plasma resonance enhancement of Raman scattering by pyridine adsorbed on silver or gold sol particles of size comparable to the excitation wavelength.* Journal of the Chemical Society, Faraday Transactions 2: Molecular and Chemical Physics, **1979**. 75: p. 790-798.

45. Qian, H., et al., *Quantum sized gold nanoclusters with atomic precision.* Accounts of chemical research, **2012**. 45(9): p. 1470-1479.

46. Pelton, M., et al., *Long-Lived Charge-Separated States in Ligand-Stabilized Silver Clusters.* Journal of the American Chemical Society, **2012**. 134(29): p. 11856-11859.

47. Kumar, S., M.D. Bolan, and T.P. Bigioni, *Glutathione-Stabilized Magic-Number Silver Cluster Compounds.* Journal of the American Chemical Society, **2010**. 132(38): p. 13141-13143.

48. Farrag, M., et al., *Preparation and Spectroscopic Properties of Monolayer-Protected Silver Nanoclusters.* The Journal of Physical Chemistry C, **2012**. 116(14): p. 8034-8043.

49.   Hostetler, M.J., et al., *Alkanethiolate Gold Cluster Molecules with Core Diameters from 1.5 to 5.2 nm: Core and Monolayer Properties as a Function of Core Size.* Langmuir, **1998**. 14(1): p. 17-30.

50.   Sugawara, A. and T. Kato, *Aragonite CaCO3 thin-film formation by cooperation of Mg2+ and organic polymer matrices.* Chemical Communications, **2000**(6): p. 487-488.

51.   Luz, G.M. and J.F. Mano, *Biomimetic design of materials and biomaterials inspired by the structure of nacre.* Philosophical Transactions of the Royal Society A: Mathematical, Physical and Engineering Sciences, **2009**. 367(1893): p. 1587-1605.

52.   Gao, H., et al., *Materials become insensitive to flaws at nanoscale: lessons from nature.* Proceedings of the national Academy of Sciences, **2003**. 100(10): p. 5597-5600.

53.   Espinosa, H.D., et al., *Tablet-level origin of toughening in abalone shells and translation to synthetic composite materials.* Nature communications, **2011**. 2: p. 173.

54.   Mayer, G., *Rigid biological systems as models for synthetic composites.* Science, **2005**. 310(5751): p. 1144-1147.

55.   Corni, I., et al., *A review of experimental techniques to produce a nacre-like structure.* Bioinspiration & biomimetics, **2012**. 7(3): p. 031001.

56.   Feng, Q.L., et al., *Crystal orientation, toughening mechanisms and a mimic of nacre.* Materials Science and Engineering: C, **2000**. 11(1): p. 19-25.

57.   Weiner, S. and H. Lowenstam, *Organization of Extracellularly Mineralized Tissues: A Comparative Study of Biological Crystal Growt.* Critical Reviews in Biochemistry and Molecular Biology, **1986**. 20(4): p. 365-408.

58.   Kato, T., *Polymer/Calcium Carbonate Layered Thin-Film Composites.* Advanced Materials, **2000**. 12(20): p. 1543-1546.

59.   Katti, K.S. and D.R. Katti, *Why is nacre so tough and strong?* Materials Science and Engineering: C, **2006**. 26(8): p. 1317-1324.

60.   Wang, R., et al., *Deformation mechanisms in nacre.* Journal of Materials Research, **2001**. 16(09): p. 2485-2493.

61.   Bonderer, L.J., A.R. Studart, and L.J. Gauckler, *Bioinspired design and assembly of platelet reinforced polymer films.* Science, **2008**. 319(5866): p. 1069-1073.

62.   Schäffer, T.E., et al., *Does Abalone Nacre Form by Heteroepitaxial Nucleation or by Growth through Mineral Bridges?* Chemistry of Materials, **1997**. 9(8): p. 1731-1740.

63.   Oaki, Y. and H. Imai, *The Hierarchical Architecture of Nacre and Its Mimetic Material.* Angewandte Chemie International Edition, **2005**. 44(40): p. 6571-6575.

64.   Tang, Z., et al., *Nanostructured artificial nacre.* Nature materials, **2003**. 2(6): p. 413-418.

65.   Podsiadlo, P., et al., *Layer-by-layer assembly of nacre-like nanostructured composites with antimicrobial properties.* Langmuir, **2005**. 21(25): p. 11915-11921.

66.   Diesen, V., et al., *Silver enhanced TiO 2 thin films: photocatalytic characterization using aqueous solutions of tris (hydroxymethyl) aminomethane.* Dalton Transactions, **2014**. 43(1): p. 344-351.

67.   Li, F.B. and X.Z. Li, *The enhancement of photodegradation efficiency using Pt–TiO2 catalyst.* Chemosphere, **2002**. 48(10): p. 1103-1111.

68.   Es-Souni, M., et al., *Brookite Formation in TiO2☐ Ag Nanocomposites and Visible-Light-Induced Templated Growth of Ag Nanostructures in TiO2.* Advanced Functional Materials, **2010**. 20(3): p. 377-385.

69.   Botha, S.S., P. Ndungu, and B.J. Bladergroen, *Physicochemical properties of oil-based nanofluids containing hybrid structures of silver nanoparticles supported on silica.* Industrial & Engineering Chemistry Research, **2011**. 50(6): p. 3071-3077.

70.   Gunawidjaja, R., et al., *Bimetallic Nanocobs: Decorating Silver Nanowires with Gold Nanoparticles.* Advanced Materials, **2008**. 20(8): p. 1544-1549.

71.   Sugimoto, T., X. Zhou, and A. Muramatsu, *Synthesis of uniform anatase TiO2 nanoparticles by gel–sol method: 4. Shape control.* Journal of Colloid and Interface Science, **2003**. 259(1): p. 53-61.

72.   Tao, A.R., et al., *Self-Organized Silver Nanoparticles for Three-Dimensional Plasmonic Crystals.* Nano Letters, **2008**. 8(11): p. 4033-4038.

73.   Castiglioni, E., P. Biscarini, and S. Abbate, *Experimental aspects of solid state circular dichroism.* Chirality, **2009**. 21(1E): p. E28-E36.

74.   Nan, J. and X.-P. Yan, *Facile fabrication of chiral hybrid organic–inorganic nanomaterial with large optical activity for selective and sensitive detection of trace Hg2+.* Chemical Communications, **2010**. 46(24): p. 4396-4398.

75.   Carrillo-Carrión, C., et al., *Selective quantification of carnitine enantiomers using chiral cysteine-capped CdSe (ZnS) quantum dots.* Analytical chemistry, **2009**. 81(12): p. 4730-4733.

76.   Liz-Marzán, L.M. and P. Mulvaney, *The Assembly of Coated Nanocrystals†.* The Journal of Physical Chemistry B, **2003**. 107(30): p. 7312-7326.

77.   Sader, J.E., et al., *Method for the calibration of atomic force microscope cantilevers.* Review of Scientific Instruments, **1995**. 66(7): p. 3789-3798.

78.   Salgueiriño-Maceira, V., F. Caruso, and L.M. Liz-Marzán, *Coated colloids with tailored optical properties.* The Journal of Physical Chemistry B, **2003**. 107(40): p. 10990-10994.

79.   Svergun, D.I. and M.H. Koch, *Small-angle scattering studies of biological macromolecules in solution.* Reports on Progress in Physics, **2003**. 66(10): p. 1735.

80.   Guinier, A., *La diffraction des rayons X aux tres petits angles: applications a l'etude de phenomenes ultramicroscopiques.* **1939**.

81.   Putnam, C.D., et al., *X-ray solution scattering (SAXS) combined with crystallography and computation: defining accurate macromolecular structures, conformations and assemblies in solution.* Quarterly reviews of biophysics, **2007**. 40(03): p. 191-285.

82.   Mertens, H.D. and D.I. Svergun, *Structural characterization of proteins and complexes using small-angle X-ray solution scattering.* Journal of structural biology, **2010**. 172(1): p. 128-141.